Measurement Report: Cloud condensation nuclei (CCN) activity in the South China Sea from shipborne observations during summer and winter of 2021: seasonal variation and anthropogenic influence.

Hengjia Ou[1], Mingfu Cai[2], Yongyun Zhang[1], Xue Ni[1], Baoling Liang[3], Qibin Sun[4,5], Shixin Mai[1], Cuizhi Sun[6], Shengzhen Zhou[1], Haichao Wang[1], Jiaren Sun[2], Jun Zhao[1]

[1]School of Atmospheric Sciences, Guangdong Province Key Laboratory for Climate Change and Natural Disaster Studies, Southern Marine Science and Engineering Guangdong Laboratory (Zhuhai), Sun Yat-sen University, Zhuhai, Guangdong 519082, China

[2]Guangdong Province Engineering Laboratory for Air Pollution Control, Guangdong Provincial Key Laboratory of Water and Air Pollution Control, South China Institute of Environmental Sciences, MEE, Guangzhou 510655, China

[3]Guangzhou Sub-branch of Guangdong Ecological and Environmental Monitoring Center, Guangzhou 510006, China

[4]Dongguan Meteorological Bureau, Dongguan, Guangdong, 523086, China

[5]Dongguan Engineering Technology Research Center of Urban Eco-Environmental Meteorology, Dongguan, Guangdong, 523086, China

[6]Southern Marine Science and Engineering Guangdong Laboratory (Zhuhai), Zhuhai, Guangdong 519082, China

Correspondence: Mingfu Cai (caimingfu@scies.org) and Jun Zhao (zhaojun23@mail.sysu.edu.cn)

Abstract

Understanding seasonal variations in cloud condensation nuclei (CCN) activity and the impact of anthropogenic emissions in marine environments is crucial for assessing climate change. This study presents findings from two shipborne observations conducted in the South China Sea (SCS) during the summer and winter of 2021. In the summer, higher particle number concentrations but lower mass concentrations of non-refractory submicron particle matters (NR-PM_4) were observed. This was attributed to the dominance of particles in the Aitken mode during summer, whereas there was a more balanced distribution of Accumulation mode and Aitken mode particles in winter. Summer particles were more hygroscopic, exhibiting higher activation ratios (ARs) at high supersaturation (SS) levels, while hygroscopicity at low SS was similar in both seasons. During the summer, three distinct periods were identified based on the air mass sources: terrestrial air masses from Luzon Island ("Luzon" period), and from the Indochinese Peninsula ("Indochinese Peninsula" period), and marine air masses. In winter, the periods were defined by terrestrial air masses from Mainland China ("Mainland China" period), a mix of Mainland China and marine air masses ("Mixed" period), and purely marine air masses. The "Luzon" period in summer exhibited the highest particle number concentration, especially in the Aitken mode, resulting in the highest CCN number concentration (N_{CCN}). Aerosol hygroscopicity was higher during the "Indochinese Peninsula" period compared to the "Luzon" period, leading to a higher AR due to the combination of higher hygroscopicity and a greater fraction of accumulation mode particles. The "Mainland China" period in winter showed a high nitrate fraction in NR-PM_4, but the inorganic fraction was similar to it in “Luzon” period, resulting in comparable hygroscopicity at low SS to the "Luzon" period. However, hygroscopicity at small particle sizes was much lower in the "Mainland China" period than in the summer periods. The "Mixed" period in winter exhibited a higher fraction of accumulation mode particles, causing a higher AR compared to the "Mainland China" period. CCN closure analysis, considering aerosol composition and mixing state, revealed that summer aerosol was primarily internally mixed, whereas smaller aerosol in winter was primarily externally mixed. The potential effect of undetected sea salt may lead to an underestimation of aerosol hygroscopicity in summer. This study highlights significant seasonal differences in aerosol properties and the impact of different types of terrestrial air masses on CCN activity in the SCS, contributing to our understanding of regional climate influences.

Formatted: Subscript

Deleted: were more

Formatted: Subscript

Formatted: Subscript

Deleted: Understanding seasonal variation in cloud condensation nuclei (CCN) activity and the impact of anthropogenic emissions in marine environments is crucial for assessing climate change. In this study, two shipborne observations in the South China Sea (SCS) during the summer and winter of 2021 were conducted. During summer, higher particle number concentrations but lower mass concentrations of non-refractory submicron particles (NR-PM_1) were observed. These differences were attributed to the dominance of particles in the Aitken mode during summer and in the accumulation mode during winter. Moreover, particles during summer were more hygroscopic with higher activation ratios (ARs) at all supersaturation (SS). Based on backward trajectory analysis, the whole campaign was classified into terrestrial and mixed air mass influence periods. Particles measured during the terrestrial period consistently exhibited lower hygroscopicity values

Deleted: . Additionally, minor variations were shown for all NR-PM_1 components under different air mass influences during summer, while the mass fraction of nitrate increased significantly under terrestrial influence during winter. Particle number size distribution (PNSD) exhibited unimodal distribution during terrestrial period and bimodal distribution during mixed air mass influence period, with winter displaying a more pronounced bimodal pattern than summer. The impact of PNSD on AR was greater than on aerosol hygroscopicity in summer, and vice versa in winter. During terrestrial period, significant variations in PNSD were observed with the offshore distance, and the largest variation was seen in Aitken mode during both summer and winter. Meanwhile, aerosol hygroscopicity shows an increasing trend with the offshore distance, which is primarily attributed to the increase of sulfate fraction during summer and the decrease of the black carbon fraction during winter. Using a single parameterized PNSD in the N_{CCN} prediction can lead to errors exceeding 100% during both summer and winter, with dominant terrestrial air masses in the SCS atmosphere, while using a constant hygroscopicity parameter would lower the errors in the N_{CCN} prediction (~15% during winter and ~10% during summer). Our study shows significant differences in aerosol properties between winter and summer seasons and highlights the influence of anthropogenic emissions on the CCN activity in the SCS.

1.Introduction

Aerosols can act as cloud condensation nuclei (CCN), influencing cloud formation, lifespan, and albedo, thus indirectly impacting global radiative balance (Fletcher et al., 2011; Albrecht, 1989). The aerosol-cloud interaction currently represents the largest uncertainty in radiative forcing within climate models, ranging from -1.7 to -0.3 W m^{-2} (IPCC, 2021). This uncertainty can be attributed to the significant spatiotemporal variability in the aerosol size distribution and the ability of atmospheric aerosol particles acting as CCN (CCN activity) (Fitzgerald, 1973). Thus, field measurements of aerosol size distribution and physicochemical properties are needed to better understand the radiative forcing exerted by atmospheric aerosol particles.

Previous studies suggest that particle number size distribution (PNSD) is a primary factor influencing CCN concentrations (Dusek et al., 2006; Rose et al., 2010; Pöhlker et al., 2016; Burkart et al., 2011). The PNSD can account for 84–96% of the variability in CCN concentrations (N_{CCN}) (Dusek et al., 2006), while CCN activities may also play a significant role in CCN concentrations (Quinn et al., 2008; Cai et al., 2018; Ovadnevaite et al., 2017; Liu et al., 2018; Crosbie et al., 2015), which are primarily governed by the particle size, chemical composition, mixing state, surface tension, and hygroscopicity (Köhler, 1936; Seinfeld and Pandis, 2016). Among these factors, the impact of hygroscopicity on CCN activities has received great attention in recent years (Petters and Kreidenweis, 2007; Ajith et al., 2022; Rose et al., 2010). Petters and Kreidenweis (2007) proposed the κ- Köhler theory based on the Köhler theory to quantify the ability of aerosol particles to absorb moisture and become CCN based on the aerosol hygroscopicity parameters (κ). Ajith et al. (2022) showed that 64% of particles can be activated as CCN when κ is equal to 0.37, whereas when κ decreases to 0.23, only 48% of particles can be activated in the tropical coastal area.

Significant seasonal variations in PNSD and hygroscopicity under both terrestrial and marine environments were observed in previous field observations, leading to the seasonal variations in N_{CCN} (Crosbie et al., 2015; Schmale et al., 2018; Burkart et al., 2011; Bougiatioti et al., 2009; Sihto et al., 2011; Leena et al., 2016; Ross et al., 2003; Gras and Keywood, 2017; Quinn et al., 2019). Crosbie et al. (2015) revealed that in the urban area of Arizona particles had larger sizes, higher hygroscopicity, and N_{CCN} was also higher during winter, while a higher abundance of smaller particles was observed during summer owing to stronger photochemical reactions. In pristine environments like mountain, coastal, and forested

Formatted: Indent: First line: 0 cm

Deleted: (Dusek et al. (2006)

regions, seasonal variations in N_{CCN} and PNSD were more pronounced than urban and rural areas (Schmale et al., 2018). Pöhlker et al. (2016) observed significant differences in N_{CCN} between the wet and dry seasons in the Amazon rainforest, while the κ values remained relatively stable. They also noted increased particle concentrations and aerosol hygroscopicity, both subject to the impact of long-range transport originating from anthropogenic emissions. Observations in marine areas during different seasons are relatively scarce compared with those in inland areas. Gras (1995) found that both particle concentration and N_{CCN} in the Southern Ocean reached their peaks during summer and gradually decrease to their valleys in winter. Quinn et al. (2019) showed that sea spray aerosols make a relatively significant contribution to N_{CCN} only during winter in the Western North Atlantic, while in other seasons, the primary contribution comes from biogenic aerosols oxidized from dimethyl sulfide (DMS). Zheng et al. (2020) revealed that sulfate dominates the particle condensational growth to CCN sizes during summer in the North Atlantic, while secondary organic aerosols played a significant role in particle growth throughout all seasons. These results indicate that CCN activity and concentration could vary in a large range during different seasons. Thus, further observations across different seasons in marine environments are needed to enhance our understanding of marine CCN activities and their seasonal variations.

The South China Sea (SCS), located in Southeast Asia and bordered by China, the Indochinese Peninsula, and Maritime Southeast Asia, is significantly influenced by air pollutants transported through terrestrial air masses. Studies have shown that these pollutants play a crucial role in determining aerosol concentration and properties in the region (Atwood et al., 2017; Xiao et al., 2017; Geng et al., 2019; Liang et al., 2021; Sun et al., 2023; Qin et al., 2024). For instance, Xiao et al. (2017) reported that 69.7% of nitrate and 57.5% of sulfate in the SCS originated from fossil fuel combustion, particularly coal burning in Chinese coastal regions. Additionally, Liang et al. (2021) and Sun et al. (2023) observed an increase in the organic fraction and concentration of submicron aerosols when the region was influenced by terrestrial air masses from Mainland China and the Indochinese Peninsula in the northern SCS. Further studies highlighted the variation in aerosol properties under different air mass influences. Atwood et al. (2017) found a significant bimodal particle distribution with a κ value of 0.65 in the southern SCS under marine air mass influence, whereas a unimodal distribution with a κ of 0.4 was observed under continental air mass influence.

The SCS experiences a typical monsoon climate with distinct seasonal wind direction changes (Wang et al., 2009). The northeast monsoon, occurring from November to March, is characterized by

stronger average wind speeds and longer period compared to the southwest monsoon, which dominates from June to August. The transitional periods occur from April to May and September to October. During the northeast monsoon, air pollutants are primarily transported to the SCS by terrestrial air masses from China (Xiao et al., 2017; Liu et al., 2014; Geng et al., 2019). In contrast, during the summer, pollutants mainly originate from terrestrial air masses from the Indochinese Peninsula and Maritime Southeast Asia (Geng et al., 2019; Liang et al., 2021; Sun et al., 2023). These varying sources of anthropogenic emissions exerts different impacts on CCN activity differently across seasons. Additionally, the high cloud fraction over the SCS varies from approximately 0.3 to 0.7 across different months, indicating that aerosol-cloud interactions in the region may differ between seasons (Lu et al., 2022). However, due to limited observational data, our understanding of seasonal variations in CCN activity in the SCS remains incomplete. Conducting comprehensive observational studies on CCN activity across different seasons is essential for improving our understanding of aerosol-cloud interactions on the SCS.

In this study, we conducted two shipborne observations in the SCS during summer (May 5–June 9, 2021) and winter (December 19–29, 2021). Our observations with online instruments focused on measuring aerosol chemical composition, PNSD, and CCN activation in the region. Our results provide valuable insights into the differences in CCN activity between winter and summer, as well as the influence of different types of terrestrial air masses on CCN activity in the SCS across different seasons.

Deleted: terrestrial transport

2. Methodology

2.1 Cruise information and onboard measurements

2.1.1 Cruise information

This study consists of two research cruises conducted during the summer and winter of 2021, respectively. These two cruises were interdisciplinary scientific expeditions, integrating fields such as marine geology, oceanography, and atmospheric environment. The primary objective in atmospheric environment was to investigate the impact of different monsoons on the atmospheric environment of the South China Sea (SCS). The summer and winter cruises were carried out respectively by the vessels "Tan Kah Kee" and "Sun Yat-sen University". The "Tan Kah Kee" is an oceanographic research vessel with a length of 77.7 meters, a beam of 16.24 meters, and a displacement of 3611 tons. The "Sun Yat-sen University" is a comprehensive oceanographic training vessel with a total length of 114.3 meters, a beam of 19.4 meters, and a displacement of 6880 tons.

The first cruise was from May 5th to June 9th, 2021. The cruise started from Xiamen Port and traversed from the northern to the central-southern South China Sea, and then circled back near Hainan Island, and finally returned to Xiamen Port. The second cruise was from December 19th to December 29th, 2021. It began from Gaolan Port in Zhuhai and reached the vicinity of Yongxing Island, and ultimately returned to Gaolan Port (Fig. 1a). Unfortunately, due to adverse weather conditions, such as strong winter monsoon winds causing poor sea conditions, and the fact that it was the first scientific deployment of the research vessel Sun Yat-sen University, the winter cruise had a shorter duration and covered a narrower spatial range compared to the summer cruise. On both cruises, most of the instruments were housed in a single compartment and the sampling lines were extended from the window of the compartment to the height of the ship's bridge (Fig. 1a).

2.1.2 Size-resolved cloud condensation nuclei activity measurement

The size-resolved CCN activity was measured with a combination of a scanning mobility particle sizer (SMPS) system and a cloud condensation nuclei counter (model CCNc-200, DMT Inc., USA), the scanning mobility CCN analysis (SMCA) method initially proposed in Moore et al. (2010). The SMPS system consisted of a differential mobility analyzer (DMA; model 3082, TSI., Inc.) and a condensation particle counter (CPC; model 3756, TSI Inc.). The SMPS and the CCNc system were used to measure PNSD and size-resolved CCN number concentration at a mobility size range of 10–500 nm and 10–593 nm in summer and winter campaign, respectively.

Formatted: No underline, Font color: Auto

Formatted: Check spelling and grammar

Deleted: set

The supersaturation (SS) of the CCNc was set at 0.2 %, 0.4 %, and 0.7 % in summer campaign and 0.1%, 0.2 %, 0.4 %, and 0.7 % in winter campaign, respectively. Before the measurements, the CCNc was calibrated with ammonium sulfate ($(NH_4)_2SO_4$) particles at each set SS. Detailed description of the instrument configuration and calibration can be found in Cai et al. (2018).

2.1.3 Aerosol chemical composition measurement

The chemical composition of atmospheric non-refractory submicron particulate matter (NR-PM_1), including sulfate, nitrate, organics, ammonium, and chloride, was measured using an online time-of-flight ACSM (ToF-ACSM; Aerodyne Inc., USA). The sampling time of the ToF-ACSM was approximately 10 min. The relative ionization efficiency (RIE) values of the instrument were calibrated using ammonium nitrate (NH_4NO_3) and ammonium sulfate ($(NH_4)_2SO_4$) both before the start and after

the completion of the campaigns. The RIE values for ammonium were 3.31 and 3.33 during the summer and winter, respectively, while the ones for sulfate were 1.02 and 0.81 during the summer and winter, respectively. The collection efficiency (CE) was determined as shown in Sun et al. (2023) and time-independent CE values were used in this study. Detailed CE calculation can be found in the supplementary (Text S1, and Fig. S1). The organic carbon (OC)/elemental carbon (EC) concentrations in $PM_{2.5}$ were measured using a semi-continuous OC/EC analyzer (Model-4, Sunset Laboratory Inc., USA) based on the thermal optical transmittance technique and detailed measurement process can be found in Sun et al. (2023). The black carbon concentrations were measured with an aethalometer (AE33, Magee Scientific).

2.1.4 Trace Gas and meteorological parameter measurements

The concentrations of trace gases (CO, O_3, SO_2, and NOx) were measured using gas monitors (T400U, T100U, and T200U; Teledyne API Inc., USA). The meteorological elements, including temperature, relative humility, wind speed, and wind direction, were measured by the combined automatic weather station onboard the vessels. During the winter cruises, meteorology data before 12.22 was missed due to the calibration for the automatic weather station before 12.22. The timeseries of meteorological data were presented in Fig. S2.

Formatted: Font: (Asian) +Body Asian (等线)

2.2 Data analysis

2.2.1 CCN activation

The size-resolved number concentration of total praticle and cloud condensation nuclei were obtained from the SMPS and CCNc thourgh the SMCA method. The activation diameter was determined by fitting the activation ratio (AR, N_{CCN}/N_{CN}) and dry diameter at each supersaturation through the following equation:

$$AR = \frac{B}{1+\left(\frac{D_P}{D_{50}}\right)^C}, \quad (1)$$

Deleted: $\frac{N_{CCN}}{N_{CN}}$

where AR is the size-resolved AR, D_P represents dry particle diameter (nm); B, C, and D_{50} are the three fitting parameters, representing the asymptote, the slope, and the inflection point of the sigmoid, respectively (Moore et al., 2010). The D_{50} parameter, also known as the critical diameter, corresponds to the particle size at which 50% of the particles are activated at a specific SS. The fitting results from SMCA method measured in this study are presented in Fig. S3.

Formatted: Font: (Asian) +Body Asian (等线)

The hygroscopicity parameter (κ) which represents CCN activity according to κ-Köhler equation is calculated as follows (Petters and Kreidenweis, 2007):

$$\kappa = \frac{4A^3}{27D_{50}^3(lnS_c)^2},\ A = \frac{4\sigma_{s/a}M_w}{RT\rho_w} \quad (2)$$

where ρ_w is the density of pure water (about 997.04 kg m^{-3} at 298.15 K), M_W is the molecular weight of water (0.018 kg mol^{-1}), $\sigma_{s/a}$ corresponds to the surface tension of the solution-air interface and is assumed to be equal to the surface tension of pure water ($\sigma_{s/a}$=0.0728 N m^{-1} at 298.15 K), R is the universal gas constant (8.314 J mol^{-1} K^{-1}), T denotes thermodynamic temperature in kelvin (298.15 K), and D_{50} is the critical diameter (in m).

2.2.2 Closure Method

According to Petters and Kreidenweis. (2007), κ can be predicted by a simple mixing rule based on chemical volume fractions:

$$\kappa_{sim} = \sum_i \varepsilon_i \kappa_i \quad (3)$$

where ε_i and κ_i are the volume fraction and hygroscopicity parameter for the specific dry component in the mixture. We obtained ε from aerosol chemical composition measured by the ToF-ACSM. In this study, κ from $(NH_4)_2SO_4$ (0.48), NH_4NO_3 (0.58), and Nacl (1.1) represent the κ of SO_4^{2-}, NO_3^-, and Cl^- provided by the ToF-ACSM (Huang et al., 2022). Besides, the κ of organic was 0.1 at this study. The density of $(NH_4)_2SO_4$, NH_4NO_3, Nacl and organic are 1769 kg m^{-3}, 1720 kg m^{-3},2165 kg m^{-3}, and 1400 kg m^{-3} (Huang et al., 2022; Gysel et al., 2007).

2.2.3 CCN concentration and activation ratio calculation

The CCN concentration (N_{CCN}) can be predicted based on particle number size distribution (PNSD) and D_{50} at a specific SS. It can be calculated by the following equation (Cai et al., 2018):

$$N_{CCN}(SS) = \int_{D_{50}(SS)}^{\infty} N_{CN}(D_P)dD_p \quad (4)$$

where N_{CCN} (SS) is CCN concentration at a specific SS, D_{50}(SS) is the activation diameter at a specific SS from the SMCA method or from closure method, and $N_{CN}(D_P)$ is the particle number concentration under specific diameter from SMPS measurement.

The AR can be calculated by:

$$AR = \frac{\int_{D_{50}(SS)}^{\infty} N_{CN}(D_P)dD_p}{\int_0^{\infty} N_{CN}(D_P)dD_p} \quad (5)$$

Formatted: Heading 3
Formatted: Font: (Default) Times New Roman
Formatted: Indent: First line: 2 ch
Formatted: Font: Times New Roman
Formatted: Font: Times New Roman, Subscript
Formatted: Font: Times New Roman
Formatted: Subscript
Formatted: Subscript
Formatted: Subscript
Formatted: Subscript
Formatted: Subscript
Formatted: Subscript
Formatted: Subscript
Formatted: Superscript
Formatted: Subscript
Formatted: Superscript
Formatted: Superscript
Formatted: Superscript
Deleted:
Formatted: Font: (Asian) +Body Asian (等线)
Deleted: 2
Deleted: 3
Deleted: from the SMCA method

It is noting that the AR here is bulk AR.

To investigate the impact of the fraction and mixing state of aerosol on N_{CCN}, two CCN simulation scheme are applied in this study (Patel et al., 2021).

(1) Internal-mixed scheme: the aerosol composition from the Tof-ACSM was assumed to be size-independent and internally mixed. All aerosol has an identical chemical compostion in the whole size range. N_{CCN} is calculated by κ_{sim} and measured PNSD according to Eq. (2), Eq. (3), and Eq. (4).

(2) External-mixed scheme: the aerosol composition from the Tof-ACSM was assumed to be size-independent and externally mixed. Four type of aerosol ($(NH_4)_2SO_4$, NH_4NO_3, Nacl and organic) are assumed to have identical concentration at each size. N_{CCN} is calculated according to the Eq. (4)

To access the simulation result from these two schemes, normalized mean bias (NMB) was used in this study:

$$NMB = \frac{\sum(N_{CCN,sim} - N_{CCN,obs})}{\sum N_{CCN,obs}} \quad (6)$$

where $N_{CCN,sim}$ is the simulated N_{CCN} from two schemes, and $N_{CCN,obs}$ is the observed N_{CCN}.

2.2.4 Backward trajectory simulation and cluster analysis

Backward trajectory calculations were performed using MeteoInfo, an open-source software (Wang, 2014) to determine potential source origins. Weekly GDAS1 (Global Data Assimilation System at a resolution of 1°) files were downloaded from the NOAA Air Resource Laboratory (ARL) website (https://www.ready.noaa.gov/gdas1.php). The calculation of backward trajectories is performed every 1hour based on the location mentioned below, generating 72-hour backward trajectories at 500m.

To clarify the sources of air masses, we applied cluster analysis in this study. During the summer cruise, we conducted cluster analysis at two key locations: the midpoint of the ship's track before the outbreak of the summer monsoon (May 5-23) and the midpoint of the track after the summer monsoon began (May 24-June 9). In the winter cruise, cluster analysis was performed at two specific locations: the ship's anchorage near Big Ten-thousand Mountain Island (December 19-22 and December 27-29) and the midpoint between Dawan Mountain Island and Yongxing Island (December 23-26).

Formatted: 公式1, Indent: First line: 0 cm
Formatted: Subscript
Formatted: Font: (Default) Times New Roman
Formatted: Subscript
Formatted: Font: (Asian) +Body Asian (等线)
Formatted: Indent: Left: 0 cm, First line: 2 ch
Deleted:
To investigate the effect of PNSD and D_{50} on N_{CCN} and AR, we defined delta N_{CCN} (ΔN_{CCN}) and delta AR (ΔAR). They are calculated by following equations:

$$\Delta N_{CCN} = \frac{N_{CCN,sim} - N_{CCN,actual}}{N_{CCN,actual}} \quad (5)$$

$$\Delta AR = \frac{N_{CCN,actual} - N_{CCN,sim}}{N_{CN,actual}} \quad (6)$$

The subscript "actual" represents the actual measured value, while the subscript "sim" represents the simulated value.
Formatted: Subscript
Formatted: Subscript
Formatted: Normal
Deleted: **2.2.3 Primary and secondary organic carbon concentration calculation**
The concentrations of primary organic carbon (POC) and secondary organic carbon (SOC) were calculated according to following equation:

$$POC = (OC/EC)_{pri} \times EC \quad (7)$$

$$SOC = OC_{total} - (OC/EC)_{pri} \times EC \quad (8)$$

where $(OC/EC)_{pri}$ is the OC/EC ratio in freshly emitted combustion aerosols, and OC_{total} and EC are available from ambient measurements. The $(OC/EC)_{pri}$ was obtained from the minimum R squared (MRS) method (Wu and Yu, 2016). The MRS approach provides more accurate estimation of SOC than $(OC/EC)_{min}$ or $(OC/EC)_{10\%}$ approach and the results obtained from the MRS method are sensitive to the magnitude of measurement uncertainty, but the bias does not exceed 23% if the uncertainty is within 20% (Wu and Yu, 2016). In this study, the $(OC/EC)_{pri}$ values were 3.65 and 0.25 in summer when affected by terrestrial air masses and terrestrial-marine mixed air masses, while they were 2.82 and 0.82 in winter when affected by terrestrial air masses and terrestrial-marine mixed air masses, respectively. The categorization method based on the influence of different air masses will be introduced in the next section.
Formatted: Font: (Asian) +Body Asian (等线)
Formatted: Indent: First line: 2 ch
Deleted:
Deleted: s
Formatted: Normal, Indent: First line: 0.71 cm, Left 0 ch

2.2.5 Data quality control

To ensure reliable atmospheric samples in the SCS and mitigate the influence of research vessel emissions, we applied the following data processing procedures (Huang et al., 2018; Cai et al., 2020; Liang et al., 2021).

Firstly, we identified organic compounds, black carbon (BC), and small particulate matter (41.4 nm particles) as indicators of ship emissions, recognizing their sudden peak values as indicative of the ship's own emissions.

Secondly, we accounted for the relative positions of the ship's chimney and the sampling tube. During the summer cruise, we excluded data corresponding to a relative wind direction (with respect to the ship's bow) between 150° and 270° and a relative wind speed (with respect to the ship's speed) of less than 2.5 m s^{-1} (Fig. S4a, Fig. S5a1, and Fig. S6a-c). During the winter cruise, we excluded data for a relative wind direction between 150° and 220° and a relative wind speed of less than 2.5 m s^{-1} (Fig. S4b, Fig. S5b1, and Figs. S6d-f).

Applying these criteria, 74.8% of the data in summer and 92.2% in winter (both at 10-minute resolution) were classified as "clean" and retained for analysis. The timeseries of data before and after quality control is shown in Fig. S7.

3. Results and discussion

3.1 CCN concentration and aerosol characteristics over SCS in summer and winter

Figure 2 presented the timeseries of PNSD (a1 and a2), NR-PM_1 mass concentrations and fractions (b1 and b2, c1 and c2), number concentrations of CCN (d1 and d2), and hygroscopicity κ-values (e1 and e2) during two campaigns in summer and winter. During the summer cruise, we observed two distinct periods around the onset of the summer monsoon. The South China Sea (SCS) summer monsoon began in the sixth pentad of May (Chao et al., 2022). In winter, the influence of the winter monsoon persisted throughout the entire observation period (Fig. 1c). Despite our measurements being limited to the northern SCS in winter, the impact of the Northeast Monsoon on the SCS was evident.

The average particle number concentration in summer (6966 cm^{-3}) was higher than in winter (4988 cm^{-3}), primarily due to the higher number concentration of Aitken-mode particles in summer (Fig. 3a-b). In summer, particles were concentrated in smaller sizes, whereas in winter, particle size distribution was

Formatted: Indent: Left: 0 cm, Right: 0 cm

Formatted: Superscript

Deleted:

Formatted: Font: Not Bold

Formatted: Heading 2, Indent: Left: 0 cm, First line: 0 cm, Right: 0 cm

Deleted: Overview

Deleted: shows

Formatted: Not Superscript/ Subscript

Formatted: Font: Times New Roman

relatively balanced between the Aitken mode (2185 cm^{-3}) and the accumulation mode (2176 cm^{-3}) (Fig. 3a-b).

The average mass concentration of NR-PM_1 was 3.76 μg m^{-3} in summer and increased to 9.39 μg m^{-3} in winter (Fig. 3c-d). In summer, the dominant aerosol component was sulfate (45.5%), followed by organics (35.8%), ammonium (12.9%), nitrate (4.0%), and chloride (1.9%) (Fig. 3c), similar to the pattern observed in the northern SCS during the summer of 2018 (Fig. 3e) (Liang et al., 2021). However, in winter, organics became the predominant aerosol component (37%), with nitrate (22.2%) replacing sulfate (18.9%) as the highest proportion of inorganic components (Fig. 3d).

The average number concentration of cloud condensation nuclei (N_{CCN}) in summer was higher than in winter at all supersaturation (SS) levels (Table 1). The absolute difference in the N_{CCN} between summer and winter was greater at high SS (ΔN_{CCN}=2099 cm^{-3} and 1865 cm^{-3} at 0.4% SS and 0.7% SS, respectively) compared to low SS (ΔN_{CCN}=341 cm^{-3} at 0.2% SS), likely due to the significant difference in Aitken-mode particles between the two seasons (Fig. 3a-b).

Aerosol hygroscopicity (κ) was similar at low SS but differed significantly at high SS between summer and winter (Table 1). The hygroscopicity pattern varied between seasons: in summer, κ increased with SS (from 0.49 to 0.72 between 0.2% SS and 0.4% SS), while in winter, κ decreased with SS (from 0.50 to 0.15 between 0.1% SS and 0.7% SS) (Fig. 3a-b). The winter κ pattern was similar to observations in the Western North Pacific (Table 1) (Kawana et al., 2020). Additionally, the winter κ values were comparable to those in Guangzhou, adjacent to the SCS, indicating that the northern SCS is influenced by air masses from Mainland China under the significant influence of the Northeast Monsoon during winter.

3.2 Anthropogenic influence on CCN concentration in different season

Based on cluster analysis, we identified periods affected by different types of air masses. In summer, three terrestrial air mass sources were confirmed: from Luzon Island (referred to as "Luzon"), Palawan Island, and the Indochinese Peninsula, along with a marine air mass source (Fig. 4a). Due to the small fraction of air masses from Palawan Island, this period was excluded from the study. Consequently, the periods affected by air masses from Luzon, the Indochinese Peninsula, and marine sources were referred to as the "Luzon" period, "Indochinese Peninsula" period, and "Marine-s" period, respectively. In winter, the identified air mass sources included Mainland China, a Mainland China-SCS mixed source (referred

Formatted: Subscript
Formatted: Subscript
Formatted: Subscript
Formatted: Subscript
Formatted: Subscript
Formatted: Normal, Indent: First line: 0.71 cm

Deleted: Based on the backward trajectories and source origins, both campaigns were classified into two periods: the period influenced by terrestrial-marine mixed air masses (31%) and the period influenced by terrestrial air masses only (69%) (Fig. S3). During the summer, terrestrial air masses primarily traverse through the Philippines region, whereas during the winter, they predominantly originate from mainland China. As shown in Fig. 2, a higher total particle number concentration during summer (11195 cm^{-3}) than during winter (6358 cm^{-3}) was obtained when the marine atmosphere was mainly influenced by terrestrial air masses. This is in line with previous studies that a higher particle number concentration of exceeding 15000 cm^{-3} was observed in Manila (the largest port city in the Philippines) than that of approximately 10000 cm^{-3} reported in Guangzhou and Hong Kong (Liu et al., 2008; Cai et al., 2017). Similar particle concentrations (2114 cm^{-3} and 1840 cm^{-3}) in winter and summer were shown when the marine atmosphere was predominantly influenced by mixed air masses. Interestingly, they are much lower than those (~3400 cm^{-3}) observed in the northern South China Sea (Cai et al., 2020), but higher than those observed in the remote SCS (975 cm^{-3}) when similar mixed influences of air masses (Atwood et al., 2017).
The average mass concentration of NR-PM_1 was 3.60 μg m^{-3} in summer and significantly increased to 18.11 μg m^{-3} in winter. However, this summer concentration was much lower than the concentrations (9.11 μg m^{-3} and 10.65 μg m^{-3}) measured in similar summer periods of 2018 and 2019 in the northern SCS (Liang et al., 2021; Sun et al., 2023). As aforementioned, the particle number concentrations were higher in summer than in winter when the atmosphere was primarily influenced by terrestrial air masses. However, the particles in summer were predominantly in the Aitken mode, resulting in a lower contribution to the mass loading than those in winter which were mainly in the accumulation mode (Fig. 3). Additionally, higher NR-PM_1 concentrations were found in both summer and winter under the influence of terrestrial air masses than mixed ones, with decreases of approximately 0.6 μg m^{-3} (from 3.84 to 3.20 μg m^{-3}) and 17 μg m^{-3} (from 23.52 to 6.32 μg m^{-3}) in summer and winter, respectively. The dramatic decrease for the latter case indicated a more pronounced impact of inland anthropogenic emissions on the aerosol mass concentration in the SCS region during winter.
As shown in Fig. 2 (d1 and d2), the N_{CCN} values at three supersaturation levels (0.2%, 0.4%, and 0.7%) in winter (1660, 2356, and 3053 cm^{-3}) were lower than those in summer (2899, 5450, and 5770 cm^{-3}), respectively. Specifically, the N_{CCN} (5450 cm^{-3}) at 0.4% SS in this study during summer is much higher than that (1544 cm^{-3}) measured at a similar SS (0.34%) in summer 2018 in the similar northern SCS region (Cai et al., 2020). This is primarily due to most of the particles being in the Aitken mode particles during summer (Figs. 3a and c). For comparison, the average total particle number concentration in summer is twice that in winter, however, no such a significant difference in CCN concentration was see ... [1]

to as “Mixed”), and a marine source (Fig. 4b). These were named as the “Mainland China” period, “Mixed” period, and “Marine-w” period, respectively.

Terrestrial air masses significantly affected the marine atmosphere in the SCS, resulting in higher NR-PM_1 mass concentration and a higher fraction of organic compounds compared to those influenced by marine air masses (Fig. 5). Additionally, the number concentration of particles (N_{CN}) in the accumulation mode and the number concentration of cloud condensation nuclei (N_{CCN}) at low supersaturation (SS) were higher during periods influenced by terrestrial air masses than those during marine air mass periods (Table 2).

In summer, the “Luzon” period had the highest N_{CN}, particularly in the Aitken mode, among all periods in both summer and winter (Fig. 6a and Table 1). The high fraction of Aitken mode particles contributed to the lowest activation ratio (AR) among the summer periods (Fig. 7a), further exacerbated by low hygroscopicity during this period (Fig. 7b). This high fraction of Aitken mode particles likely indicates a high fraction of primary organic aerosol, which lowers aerosol hygroscopicity.

The N_{CN} during the “Indochinese Peninsula” period was lower than during the “Marine-s” period (Table 2). This difference was mainly due to the variation of Aitken mode particles, while accumulation mode particles were higher during the “Indochinese Peninsula” period than in “Marine-s” period (Table 2). The “Marine-s” period occurred primarily during the transition before the summer monsoon onset, when wind direction shifted from east (Luzon Island direction) to southwest (Indochinese Peninsula direction). Anthropogenic emissions from Luzon Island still affected the marine atmosphere, leading to higher concentrations of Aitken mode particles compared to the “Indochinese Peninsula” period (Table 2). The higher fraction of accumulation mode particles and higher hygroscopicity during the “Indochinese Peninsula” period resulted in a higher AR compared to the “Luzon” period. Despite a higher organic fraction in NR-PM_1 during the “Indochinese Peninsula” period (Fig. 5), hygroscopicity was still higher due to a higher oxidation degree of organics, indicated by a higher m/z 44 to 43 ratio (5.87 compared to 5.60 in the “Luzon” period) (Lambe et al., 2011; Jimenez et al., 2009). Additionally, higher wind speeds during this period (7.26 m s^{-1} compared to 3.18 m s^{-1} in the “Luzon” period) leaded a higher fraction of sea salt (Huang et al., 2022), resulting a higher aerosol hygroscopicity. Unfortunately, owing to instrument limit, sea salt cannot be detected by the ToF-ACSM.

In winter, nitrate had the highest fraction in NR-PM_1 (25.4%) during the “Mainland China” period among other periods. Due to similar hygroscopicity between nitrate and sulfate and similar inorganic

Formatted: Subscript
Formatted: Subscript
Formatted: Subscript
Formatted: Subscript
Formatted: Subscript
Formatted: Subscript
Formatted: Superscript
Formatted: Subscript

fractions between the "Mainland China" and "Luzon" periods, κ at 0.2% SS was comparable (0.30 and 0.33, respectively) (Fig. 7b). However, aerosol hygroscopicity at small sizes was much lower in the "Mainland China" period than in the "Luzon" period (Fig. 7b), contributing to the low AR in the "Mainland China" period (Fig. 7a). This lower hygroscopicity could be due to lower sulfate concentration, oxidized by DMS, in winter than in summer, as higher sea surface temperatures in summer (29.3°C) compared to winter (18.0°C) promote DMS production by phytoplankton (Bates et al., 1987). The similar fractions of Aitken mode and accumulation particles indicated that PNSD could not fully explain the low AR in the "Mainland China" period. Lower N_{CN} and AR in the "Mainland China" period compared to the "Luzon" period resulted in a lower N_{CCN}.

During the "Mixed" period, the N_{CCN} was lower than in the "Mainland China" period, attributed to decreased N_{CN} (Table 2). However, particles were primarily concentrated in the accumulation mode, distinct from other terrestrial air mass periods (Fig. 6), leading to a significantly higher AR than the "Mainland China" period. Organic aerosol hygroscopicity was higher during the "Mixed" period than the "Mainland China" period, supported by a higher m/z 44 to 43 ratio (3.88 compared to 3.10 in the "Mainland China" period), explaining the higher hygroscopicity despite a higher organic fraction in NR-PM_1. Additionally, lower BC concentration in the "Mixed" period (1.20 μg m^{-3} compared to 2.25 μg m^{-3} in the "Mainland China" period) suggested a lower fraction of BC, which was hydrophobic. Higher wind speeds in the "Mixed" period (10.77 m s^{-1} compared to 7.14 m s^{-1} in the "Mainland China" period) could increase sea salt fraction, further enhancing aerosol hygroscopicity.

3.3 CCN closure analysis

CCN closure study was widely applied to investigate the impacts of different factors on the CCN activity (Patel et al., 2021; Cai et al., 2018; Meng et al., 2014; Deng et al., 2013). In this study, two schemes considering aerosol composition and mixing state based on CCN closure method mentioned in 2.2.3 were applied. The fitting parameter and coefficient of determination (R^2) was shown in Table 3 and the fitting plots from two schemes were shown in Fig. S8 and Fig. S9. Besides, the NMB from these two schemes was presented in Fig. 8.

In summer, the NMB always lower than 0, which indicated that simulated aerosol hygroscopicity was lower than observed value (Fig. 8). Sea salt which cannot be detected by the ToF-ACSM may account for higher fraction in summer due to low aerosol concentration in summer (Fig. 3c), resulting in

Formatted: Font: Times New Roman
Formatted: Subscript
Formatted: Subscript
Formatted: Subscript
Formatted: Indent: First line: 2 ch
Formatted: Subscript
Formatted: Subscript
Formatted: Superscript
Formatted: Superscript

the underestimation of aerosol hygroscopicity. The NMB exhibits different trends with changes in SS in "Luzon" and "Indochinese Peninsula" period. Better fitting result appeared in high SS in "Indochinese Peninsula" period, while it appeared in low SS in "Luzon" period (Fig. 8), which indicated that aerosol fraction had different trend as particle size increased in these two periods. Besides, "Internal-mixed" scheme had more precious result than it in "External-mixed" scheme in summer (Fig. 8), suggesting the aerosol was primary internally mixed in summer.

In winter, the "External-mixed" scheme always showed a better result than "Internal-mixed" scheme at high SS (0.4% SS and 0.7% SS), indicating that particles in small size were mainly externally mixed. Considering the low hygroscopicity of small-sized particles in winter, it is likely that a significant fraction of these particles consists of externally mixed BC, which probably originated from fresh anthropogenic emissions and remains unmixed with other inorganic salts and organics. As BC ages, inorganic and organic components adhere to it, which would lead to the increase of diameter and particles tended to be internally mixed (Sarangi et al., 2019). This transition resulted in higher hygroscopicity in large-sized particle compared to the smaller-sized particles. Besides, overestimation of aerosol hygroscopicity at high SS could be owing to a higher fraction of non- or less- hygroscopic component (such as organic and BC) at small particle sizes. The predicted N_{CCN} at 0.1% SS are 10%-20% lower than the observed concentrations, whereas the predicted value at 0.2% SS more closely aligns with the observed concentrations (Fig. 8). It could be owing to the higher fraction of sea salt at larger particle size. However, due to instrument limitations, black carbon and sea salt cannot be detected by the ToF-ACSM. More observations containing sea salt and black carbon are needed in the future to better assess their effects on aerosol hygroscopicity in SCS. In addition, further study size-resolved aerosol composition can also enhance the understanding on CCN activity in the SCS.

4. Conclusion

In this study, we investigated the seasonal variations of cloud condensation nuclei (CCN) activity in the South China Sea (SCS) and explored the impact of anthropogenic emissions. Shipborne observations were conducted during the summer (May 5–June 9) and winter (December 19–29) of 2021. We measured CCN activity, chemical composition, and particle number size distribution (PNSD) using several onboard instruments, including a ToF-ACSM, a CCNc, an SMPS, and an AE33. Observations

Formatted: Indent: First line: 0 ch

Formatted: Font: Bold, (Intl) +Headings (等线 Light), Subscript

Deleted: 3.3 Differences in the CCN activation ratio during different seasons

The CCN activation ratio (AR), which quantifies the number fraction of aerosol particles capable of acting as CCN at a specific supersaturation level, is an important parameter for characterizing the CCN activity (Dusek et al., 2006). In addition, AR is also a useful parameter in the CCN prediction (Pruppacher, 2010; Deng et al., 2013). Figure 6 illustrates the variations in AR and N_{CCN} under the influence of different air masses during different seasons. The median AR values were higher in summer (0.39, 0.67, and 0.85 at 0.2%, 0.4%, and 0.7% SS, respectively) than in winter (0.21, 0.36, 0.49, and 0.64 at 0.1%, 0.2%, 0.4%, and 0.7% SS, respectively). In summer under terrestrial air masses, the ARs (0.34–0.81 at 0.2%–0.7% SS) in this study were lower than those (0.49–0.85 at 0.18%–0.59% SS) in a previous study in the same region (Cai et al., 2020), but higher than those (0.18–0.48 at 0.11%–0.60% SS) in the Western North Pacific (Kawana et al., 2022). However, under mixed air masses, the AR values were higher than those (0.31–0.71 at 0.18%–0.59% SS) reported in Cai et al. (2020) and close to those (0.42–0.85 at 0.11%–0.60% SS) in the Western North Pacific (Kawana et al., 2022). In winter under terrestrial air masses, the AR values were in a range of 0.14 to 0.59 at 0.1%–0.7% SS, consistent with those measured in the Guangzhou (0.26–0.64 at 0.1%–0.7% SS) and Hong Kong (0.16–0.65 at 0.15%–0.7% SS) (Cai et al., 2018; Meng et al., 2014).

The differences of AR between different seasons under different air masses could be attributed to different PNSD and hygroscopicity. When the PNSD concentrates particles in the size range beyond the D_{50}, more particles can be activated as CCN, leading to higher ARs. Meanwhile, more hygroscopic particles intend to have smaller D_{50} values with which more particles can be activated. Previous studies showed that the influence of the above two factors may vary under different environments. The PNSD played a more important role in most cases in continental area (Dusek et al., 2006; Tao et al.,2021), while hygroscopicity can also have significant effects in some environments, such as boreal forest and coastal area (Roldin et al., 2019, Bougiatioti et al., 2016). Here, we investigate the relative importance of aerosol PNSD and chemical composition (hence hygroscopicity) in the SCS during different seasons under different air masses. We define ΔAR as the difference between the actual and estimated AR using Eq. (7), following a procedure illustrated in Fig. S8. AR was calculated using Eq. (4) based on the average D_{50} and the PNSD obtained during different seasons and periods (Fig. S8). Figure 7 shows that the ΔAR values at 0.2%–0.7% SS between summer and winter due to D_{50} were from -22% to 29%, while they were from -10% to 12% due to PNSD, indicating more significant influence of D_{50} than PNSD on N_{CCN} in the South China. In fact, the peak diameters of PNSD during both winter and summer are around 70 nm, and their variations are relatively small compared to the changes in D_{50} (Fig. S9).

We further investigate the influence of PNSD and hygroscopicity on AR under different air masses in the same season. In summer, the influence of PNSD on the AR can reach 6.0% to 9.8% between different periods (Figs. 7 b1 and c1), with the most significant impact at 0.2% SS (D_{50} > 90 nm). This can be attributed to the fact that large vari... [2]

included periods before and after the summer monsoon outbreak and periods influenced by the winter monsoon.

Our results show that particle number concentration (N_{CN}) and CCN number concentration (N_{CCN}) were higher in summer than in winter, while the mass concentration of non-refractory submicron particulate matter (NR-PM_1) was lower in summer. This can be attributed to the predominance of Aitken mode particles in summer, compared to the higher concentration of accumulation mode particles in winter. Additionally, aerosol hygroscopicity and activation ratio (AR) were found to be higher in summer than in winter.

Backward trajectory and cluster analysis identified distinct air mass influences. In summer, we confirmed periods affected by terrestrial air masses from Luzon Island ("Luzon" period) and the Indochinese Peninsula ("Indochinese Peninsula" period), as well as a period influenced by marine air masses ("Marine-s" period). In winter, the periods were influenced by terrestrial air masses from Mainland China ("Mainland China" period), mixed air masses from Mainland China and marine sources ("Mixed" period), and marine air masses ("Marine-w" period). Periods influenced by terrestrial air masses showed higher NR-PM_1 mass concentration, organic fraction, and N_{CCN}, especially at low supersaturation (SS), compared to those influenced by marine air masses.

During the "Luzon" period, high N_{CCN} was observed, attributed to high N_{CN}, especially in the Aitken mode. This high concentration in the Aitken mode resulted in a low AR at 0.2% SS, indicating a higher fraction of primary organic aerosol with low hygroscopicity. This caused lower overall hygroscopicity compared to other summer periods. The lower ratio of m/z 44 to 43 also suggested a lower oxidation degree of organics in this period. In the "Indochinese Peninsula" period, a higher particle fraction in the accumulation mode compared to the "Luzon" period led to a higher AR, combined with increased hygroscopicity.

In winter, the "Mainland China" period showed a high nitrate fraction in NR-PM_1. Similar inorganic fractions in NR-PM1 between the "Mainland China" and "Luzon" periods resulted in similar aerosol hygroscopicity at low SS (0.2% SS). However, at higher SS (0.4% SS and 0.7% SS), the "Mainland China" period exhibited much lower hygroscopicity, causing a lower AR at high SS. During the "Mixed" period, accumulation mode particles predominated, leading to a high AR. This indicated an aging process during transport, with more oxidized organics and higher aerosol hygroscopicity. The lower black carbon

Formatted: Subscript
Formatted: Subscript
Formatted: Subscript
Formatted: Subscript
Formatted: Subscript
Formatted: Subscript
Formatted: Subscript
Formatted: Subscript
Formatted: Subscript

(BC) fraction and the higher sea salt fraction from high wind speed contributed to higher hygroscopicity in the "Mixed" period compared to the "Mainland China" period, despite the high organic fraction.

The CCN closure analysis, considering aerosol composition and mixing state, revealed that aerosols in summer were primarily internally mixed, while in winter, small-sized aerosols were primarily externally mixed. This distinction is crucial for climate models predicting N_{CCN} in the SCS. The underestimation of aerosol hygroscopicity in summer suggests that the effect of sea salt should be considered.

Our study highlights significant seasonal differences in CCN activity in the SCS and the influence of different types of terrestrial air masses. Future measurements including size-resolved aerosol composition and obtain more precise measurements of BC and sea salt are needed to better understanding CCN activity in this region. Additionally, our observation in winter focused on the CCN activity over the northern SCS, while the influence of air masses from Mainland China in remote SCS was still unclear. Further observations in remote SCS areas could help clarify the anthropogenic influence during winter under the effect of the winter monsoon.

Data availability. Data from the measurements are available at https://doi.org/10.6084/m9.figshare.25472545 (Ou et al., 2024).

Supplement. The supplement related to this article is available online at xxx.

Author contributions. **HO, MC, and JZ** designed the research. **YZ, XN, BL, and CS** performed the measurements. **HO, MC, QS, and SM** analyzed the data. **SZ and HW** provided useful comment on the paper. **HO, MC,** and **JZ** wrote the paper with contributions from all co-authors.

Competing interests. The authors declare that they have no conflict of interest.

Formatted: Font: Not Bold, Subscript

Formatted: Normal, Indent: First line: 1.5 ch

Formatted: Font: (Asian) +Body Asian (等线)

Deleted: In this study, we investigated the seasonal variations of CCN activity in the SCS and explored the impact of anthropogenic emissions, based on shipborne observations conducted during the summer (May 5–June 9) and winter (December 19–29) of 2021. CCN activity, chemical composition, and particle number size distribution (PNSD) over the SCS were measured using several onboard instruments including a ToF-ACSM, a CCNc, an SMPS, an OC/EC analyzer, an AE33, and several monitors for trace gases (i.e., SO_2, NOx, CO, and O_3). Our results show that the particle number concentration (N_{CN}) and CCN number concentration (N_{CCN}) during summer were higher than those during winter, while the NR-PM_1 mass concentration was lower in summer, which can be attributed to the predominance of the Aitken mode particles in summer than a significant higher concentration of the accumulation mode particles during winter. Additionally, the aerosol hygroscopicity was found to be higher in summer than in winter, likely due to the enhanced terrestrial air masses and the increased proportions of black carbon and decreased sulfate concentrations from DMS oxidation.
Based on backward trajectories, both campaigns could be divided into two periods: period affected by terrestrial air masses and period affected by both terrestrial and marine (mixed) air masses. In summer, the terrestrial air masses originate primarily from the Philippines, whereas in winter, they predominantly originate from the PRD region of China. The hygroscopicity under terrestrial air masses was lower than that under mixed air masses during both seasons, and it was similar to that observed in the PRD region during winter. The PNSD distribution exhibited a unimodal pattern under the terrestrial air masses, whereas a bimodal pattern was observed under the mixed air masses. During winter, the N_{CCN} values were higher under terrestrial air masses in contrast to higher AR values under mixed air masses. During summer, the AR ratio was primarily influenced by PNSD, whereas during winter, it was more strongly influenced by aerosol hygroscopicity than by PNSD.
Our study demonstrated significant variations in the aerosol concentration and physicochemical properties with increasing offshore distances under terrestrial air masses during both summer and winter. The decreasing trends observed in various gas concentrations (NO_X and CO) with increasing offshore distances suggest a diminishing influence of anthropogenic emissions. The aerosol hygroscopicity increased with increasing offshore distances, primarily due to the decrease of the organic fraction, the oxidation degree of the organic component, the decreased proportions of black carbon, and the increased sulfate ratio. We found that the predicted CCN concentrations nearshore based on a single PNSD under terrestrial air masses could lead to significant error (15%–360%). In contrast, using a representative hygroscopicity parameter value nearshore can reduce the error in predicting N_{CCN} (5%–10%). Hence, the PNSD had a greater impact on N_{CCN} prediction than hygroscopicity. Our study highlights the significant differences of CCN activity during summer and winter in the SCS and significant influence of anthropogenic emissions on the CCN activity. Future studies should include observations during spring and autumn to explore the impact of mixing state on aer... [3]

Financial support. This work was supported by National Natural Science Foundation of China (NSFC) (Grant No. 42305123 and 42175115) and Basic and Guangzhou Applied Basic Research Foundation (Grant No. 2023A1515012240 and 2024A1515030221).

Acknowledgements. Additional support from the crew of the vessels "Tan Kah Kee" and "Sun Yat-sen University" is greatly acknowledged.

Deleted: of Guangdong Province

Reference

Ajith T. C, Kompalli, S. K., and Babu, S. S.: Role of Aerosol Physicochemical Properties on Aerosol Hygroscopicity and Cloud Condensation Nuclei Activity in a Tropical Coastal Atmosphere, ACS Earth Space Chem, 6, 1527-1542, doi:https://doi.org/10.1021/acsearthspacechem.2c00044, 2022.

Albrecht, B. A.: Aerosols, cloud microphysics, and fractional cloudiness, Science, 245, 1227-1230, doi:https://doi.org/10.1126/science.245.4923.1227, 1989.

Atwood, S. A., Reid, J. S., Kreidenweis, S. M., Blake, D. R., Jonsson, H. H., Lagrosas, N. D., Xian, P., Reid, E. A., Sessions, W. R., and Simpas, J. B.: Size-resolved aerosol and cloud condensation nuclei (CCN) properties in the remote marine South China Sea - Part 1: Observations and source classification, Atmos. Chem. Phys., 17, 1105-1123, doi:https://doi.org/10.5194/acp-17-1105-2017, 2017.

Bates, T. S., Cline, J. D., Gammon, R. H., and Kelly-Hansen, S. R.: Regional and seasonal variations in the flux of oceanic dimethylsulfide to the atmosphere, J. Geophys. Res. Oceans, 92, 2930-2938, doi:https://doi.org/10.1029/JC092iC03p02930, 1987.

Bougiatioti, A., Fountoukis, C., Kalivitis, N., Pandis, S. N., Nenes, A., and Mihalopoulos, N.: Cloud condensation nuclei measurements in the marine boundary layer of the eastern Mediterranean: CCN closure and droplet growth kinetics, Atmos. Chem. Phys., 9, 7053-7066, doi:https://doi.org/10.5194/acp-9-7053-2009, 2009.

Burkart, J., Steiner, G., Reischl, G., and Hitzenberger, R.: Long-term study of cloud condensation nuclei (CCN) activation of the atmospheric aerosol in Vienna, Atmos Environ, 45, 5751-5759, doi:https://doi.org/10.1016/j.atmosenv.2011.07.022, 2011.

Cai, M., Tan, H., Chan, C. K., Mochida, M., Hatakeyama, S., Kondo, Y., Schurman, M. I., Xu, H., Li, F., Shimada, K., Li, L., Deng, Y., Yai, H., Matsuki, A., Qin, Y., and Zhao, J.: Comparison of Aerosol Hygroscopcity, Volatility, and Chemical Composition between a Suburban Site in the Pearl River Delta Region and a Marine Site in Okinawa, Aerosol Air Qual Res, 17, 3194-3208, doi:https://doi.org/10.4209/aaqr.2017.01.0020, 2017.

Cai, M. F., Liang, B. L., Sun, Q. B., Zhou, S. Z., Chen, X. Y., Yuan, B., Shao, M., Tan, H. B., and Zhao, J.: Effects of continental emissions on cloud condensation nuclei (CCN) activity in the northern South China Sea during summertime 2018, Atmos. Chem. Phys., 20, 9153-9167, doi:https://doi.org/10.5194/acp-20-9153-2020, 2020.

Deleted: Bhattu, D., Tripathi, S. N., and Chakraborty, A.: Deriving aerosol hygroscopic mixing state from size-resolved CCN activity and HR-ToF-AMS measurements, Atmos Environ, 142, 57-70, doi:https://doi.org/10.1016/j.atmosenv.2016.07.032, 2016.

Deleted: Bougiatioti, A., Bezantakos, S., Stavroulas, I., Kalivitis, N., Kokkalis, P., Biskos, G., Mihalopoulos, N., Papayannis, A., and Nenes, A.: Biomass-burning impact on CCN number, hygroscopicity and cloud formation during summertime in the eastern Mediterranean, Atmospheric Chemistry and Physics, 16, 7389-7409, doi:https://doi.org/10.5194/acp-16-7389-2016, 2016.

Cai, M. F., Tan, H. B., Chan, C. K., Qin, Y. M., Xu, H. B., Li, F., Schurman, M. I., Liu, L., and Zhao, J.: The size-resolved cloud condensation nuclei (CCN) activity and its prediction based on aerosol hygroscopicity and composition in the Pearl Delta River (PRD) region during wintertime 2014, Atmos. Chem. Phys., 18, 16419-16437, doi:https://doi.org/10.5194/acp-18-16419-2018, 2018.

Chao, Q., Xiao, C., Li, w., Wang, L., Sun, L., Chen, X., Chen, Y., Li, Y., Gao, G., Liu, Y., Zhang, D., Ai, W., Chen, Y., Cui, T., Dai, T., Feng, A., Guo, Y., Huang, D., Jiang, Y., Li, D., Li, M., Liu, B., Liu, Y., Lv, Z., Mei, m., Wang, Q., Wang, Y., Yin, Y., Zeng, H., Zhang, Y., Zhai, J., Zhao, L., Zhi, R., Zhong, H., Zhou, X., Zhou, X., Zhu, X., and Wu, H.: China Climate Bulletin (2022), China Meteorological Administration, https://www.cma.gov.cn/zfxxgk/gknr/qxbg/202303/t20230324_5396394.html, 2022.

Choi, Y., Rhee, T. S., Collett, J. L., Park, T., Park, S.-M., Seo, B.-K., Park, G., Park, K., and Lee, T.: Aerosol concentrations and composition in the North Pacific marine boundary layer, Atmos Environ., 171, 165-172, doi:https://doi.org/10.1016/j.atmosenv.2017.09.047, 2017.

Crosbie, E., Youn, J. S., Balch, B., Wonaschutz, A., Shingler, T., Wang, Z., Conant, W. C., Betterton, E. A., and Sorooshian, A.: On the competition among aerosol number, size and composition in predicting CCN variability: a multi-annual field study in an urbanized desert, Atmos Chem Phys, 15, 6943-6958, doi:https://doi.org/10.5194/acp-15-6943-2015, 2015.

Deng, Z. Z., Zhao, C. S., Ma, N., Ran, L., Zhou, G. Q., Lu, D. R., and Zhou, X. J.: An examination of parameterizations for the CCN number concentration based on in situ measurements of aerosol activation properties in the North China Plain, Atmos. Chem. Phys., 13, 6227-6237, doi:https://doi.org/10.5194/acp-13-6227-2013, 2013.

Dusek, U., Frank, G. P., Hildebrandt, L., Curtius, J., Schneider, J., Walter, S., Chand, D., Drewnick, F., Hings, S., Jung, D., Borrmann, S., and Andreae, M. O.: Size matters more than chemistry for cloud-nucleating ability of aerosol particles, Science, 312, 1375-1378, doi:https://doi.org/10.1126/science.1125261, 2006.

Fitzgerald, J. W.: Dependence of the Supersaturation Spectrum of CCN on Aerosol Size Distribution and Composition, J Atmos Sci, 30, 628-634, doi:https://doi.org/10.1175/1520-0469(1973)030, 1973.

Fletcher, Squires, I. b. P., and Bowen, F. b. E. G.: The Physics of Rainclouds, 2011.

Geng, X. F., Zhong, G. C., Li, J., Cheng, Z. B., Mo, Y. Z., Mao, S. D., Su, T., Jiang, H. Y., Ni, K. W., and Zhang, G.: Molecular marker study of aerosols in the northern South China Sea: Impact of atmospheric

Formatted: Normal

Formatted: Font: (Asian) +Body Asian (等线)

Deleted: Dusek, U., Frank, G. P., Curtius, J., Drewnick, F., Schneider, J., Kürten, A., Rose, D., Andreae, M. O., Borrmann, S., and Pöschl, U.: Enhanced organic mass fraction and decreased hygroscopicity of cloud condensation nuclei (CCN) during new particle formation events, Geophys Res Lett, 37, doi:https://doi.org/10.1029/2009GL040930, 2010.

Deleted: Frossard, A. A., Russell, L. M., Burrows, S. M., Elliott, S. M., Bates, T. S., and Quinn, P. K.: Sources and composition of submicron organic mass in marine aerosol particles, J Geophys Res-Atmos, 119, 12977-13003, doi:https://doi.org/10.1002/2014jd021913, 2014.

outflow from the Indo-China Peninsula and South China, Atmos Environ, 206, 225-236, doi:https://doi.org/10.1016/j.atmosenv.2019.02.033, 2019.

Gras, J. L.: CN, CCN and particle size in Southern Ocean air at Cape Grim, Atmos Res, 35, 233-251, doi:https://doi.org/10.1016/0169-8095(94)00021-5, 1995.

Gras, J. L. and Keywood, M.: Cloud condensation nuclei over the Southern Ocean: wind dependence and seasonal cycles, Atmos. Chem. Phys., 17, 4419-4432, doi:https://doi.org/10.5194/acp-17-4419-2017, 2017.

Gysel, M., Crosier, J., Topping, D. O., Whitehead, J. D., Bower, K. N., Cubison, M. J., Williams, P. I., Flynn, M. J., McFiggans, G. B., and Coe, H.: Closure study between chemical composition and hygroscopic growth of aerosol particles during TORCH2, Atmos. Chem. Phys., 7, 6131-6144, doi:https://doi.org/10.5194/acp-7-6131-2007, 2007.

Huang, S., Wu, Z. J., Poulain, L., van Pinxteren, M., Merkel, M., Assmann, D., Herrmann, H., and Wiedensohler, A.: Source apportionment of the organic aerosol over the Atlantic Ocean from 53 degrees N to 53 degrees S: significant contributions from marine emissions and long-range transport, Atmos. Chem. Phys., 18, 18043-18062,doi: 10.5194/acp-18-18043-2018, 2018.

Huang, S., Wu, Z., Wang, Y., Poulain, L., Höpner, F., Merkel, M., Herrmann, H., and Wiedensohler, A.: Aerosol Hygroscopicity and its Link to Chemical Composition in a Remote Marine Environment Based on Three Transatlantic Measurements, Environ. Sci. Technol, 56, 9613-9622, doi:https://doi.org/10.1021/acs.est.2c00785, 2022.

Ipcc: Annex I: Observational Products [Trewin, B. (ed.)], in: Climate Change 2021: The Physical Science Basis. Contribution of Working Group I to the Sixth Assessment Report of the Intergovernmental Panel on Climate Change, edited by: Masson-Delmotte, V., Zhai, P., Pirani, A., Connors, S. L., Péan, C., Berger, S., Caud, N., Chen, Y., Goldfarb, L., Gomis, M. I., Huang, M., Leitzell, K., Lonnoy, E., Matthews, J. B. R., Maycock, T. K., Waterfield, T., Yelekçi, O., Yu, R., and Zhou, B., Cambridge University Press, Cambridge, United Kingdom and New York, NY, USA, 2061–2086, https://doi.org/10.1017/9781009157896.015, 2021.

Jimenez, J. L., Canagaratna, M. R., Donahue, N. M., Prevot, A. S., Zhang, Q., Kroll, J. H., DeCarlo, P. F., Allan, J. D., Coe, H., Ng, N. L., Aiken, A. C., Docherty, K. S., Ulbrich, I. M., Grieshop, A. P., Robinson, A. L., Duplissy, J., Smith, J. D., Wilson, K. R., Lanz, V. A., Hueglin, C., Sun, Y. L., Tian, J., Laaksonen, A., Raatikainen, T., Rautiainen, J., Vaattovaara, P., Ehn, M., Kulmala, M., Tomlinson, J. M., Collins, D.

Deleted: H.R. Pruppacher, J. D. K.: Microphysics of Clouds and Precipitation, Atmospheric and Oceanographic Sciences Library, Springer Dordrecht, XXII, 954 pp., https://doi.org/10.1007/978-0-306-48100-0, 2010.

Formatted: Font: (Asian) +Body Asian (等线)

Deleted: Jayachandran, V., Safai, P. D., Soyam, P. S., Malap, N., Bankar, S. P., Varghese, M., and Prabha, T. V.: Characterization of carbonaceous aerosols during the Indian summer monsoon over a rain-shadow region, Air Qual Atmos Hlth, 15, 1713-1728, doi:https://doi.org/10.1007/s11869-022-01211-1, 2022.

R., Cubison, M. J., Dunlea, E. J., Huffman, J. A., Onasch, T. B., Alfarra, M. R., Williams, P. I., Bower, K., Kondo, Y., Schneider, J., Drewnick, F., Borrmann, S., Weimer, S., Demerjian, K., Salcedo, D., Cottrell, L., Griffin, R., Takami, A., Miyoshi, T., Hatakeyama, S., Shimono, A., Sun, J. Y., Zhang, Y. M., Dzepina, K., Kimmel, J. R., Sueper, D., Jayne, J. T., Herndon, S. C., Trimborn, A. M., Williams, L. R., Wood, E. C., Middlebrook, A. M., Kolb, C. E., Baltensperger, U., and Worsnop, D. R.: Evolution of organic aerosols in the atmosphere, Science, 326, 1525-1529, doi:https://doi.org/10.1126/science.1180353, 2009.

Kawana, K., Miyazaki, Y., Omori, Y., Tanimoto, H., Kagami, S., Suzuki, K., Yamashita, Y., Nishioka, J., Deng, Y. G., Yai, H., and Mochida, M.: Number-Size Distribution and CCN Activity of Atmospheric Aerosols in the Western North Pacific During Spring Pre-Bloom Period: Influences of Terrestrial and Marine Sources, J Geophys Res-Atmos, 127, e2022JD036690, doi:https://doi.org/10.1029/2022JD036690, 2022.

Köhler, H.: The nucleus in and the growth of hygroscopic droplets, Trans. Faraday Soc., 32, 1152-1161, doi:https://doi.org/10.1039/TF9363201152, 1936.

Lambe, A. T., Onasch, T. B., Massoli, P., Croasdale, D. R., Wright, J. P., Ahern, A. T., Williams, L. R., Worsnop, D. R., Brune, W. H., and Davidovits, P.: Laboratory studies of the chemical composition and cloud condensation nuclei (CCN) activity of secondary organic aerosol (SOA) and oxidized primary organic aerosol (OPOA), Atmos. Chem. Phys., 11, 8913-8928, doi:https://doi.org/10.5194/acp-11-8913-2011, 2011.

Leena, P. P., Pandithurai, G., Anilkumar, V., Murugavel, P., Sonbawne, S. M., and Dani, K. K.: Seasonal variability in aerosol, CCN and their relationship observed at a high altitude site in Western Ghats, Meteorol Atmos Phys, 128, 143-153, doi:https://doi.org/10.1007/s00703-015-0406-0, 2016.

Liang, B., Cai, M., Sun, Q., Zhou, S., and Zhao, J.: Source apportionment of marine atmospheric aerosols in northern South China Sea during summertime 2018, Environ. Pollut, 289, 117948, doi:https://doi.org/10.1016/j.envpol.2021.117948, 2021.

Liu, P., Song, M., Zhao, T., Gunthe, S. S., Ham, S., He, Y., Qin, Y. M., Gong, Z., Amorim, J. C., Bertram, A. K., and Martin, S. T.: Resolving the mechanisms of hygroscopic growth and cloud condensation nuclei activity for organic particulate matter, Nat. Commun, 9, 4076, doi:https://doi.org/10.1038/s41467-018-06622-2, 2018.

Liu, X. and Wang, J.: How important is organic aerosol hygroscopicity to aerosol indirect forcing?, Environ. Res. Lett, 5, 044010, doi:https://doi.org/10.1088/1748-9326/5/4/044010, 2010.

Deleted: Kuang, Y., Xu, W., Tao, J., Ma, N., Zhao, C., and Shao, M.: A Review on Laboratory Studies and Field Measurements of Atmospheric Organic Aerosol Hygroscopicity and Its Parameterization Based on Oxidation Levels, Curr. Pollut. Rep, 6, 410-424, doi:https://doi.org/10.1007/s40726-020-00164-2, 2020.

Deleted: Liu, S., Hu, M., Wu, Z., Wehner, B., Wiedensohler, A., and Cheng, Y.: Aerosol number size distribution and new particle formation at a rural/coastal site in Pearl River Delta (PRD) of China, Atmos Environ, 42, 6275-6283, doi:https://doi.org/https://doi.org/10.1016/j.atmosenv.2008.01.063, 2008.

Liu, Y., Sun, L., Zhou, X., Luo, Y., Huang, W., Yang, C., Wang, Y., and Huang, T.: A 1400-year terrigenous dust record on a coral island in South China Sea, Sci Rep, 4, 4994, doi:https://doi.org/10.1038/srep04994, 2014.

Lu, W., Yang, S., Zhu, W., Li, X., Cui, S., Luo, T., Han, L., and Shi, J.: Evaluation of High Cloud Product of ECMWF Over South China Sea Using CALIOP, Earth Space Sci, 9, e2021EA002113, doi:https://doi.org/10.1029/2021ea002113, 2022.

Meng, J. W., Yeung, M. C., Li, Y. J., Lee, B. Y. L., and Chan, C. K.: Size-resolved cloud condensation nuclei (CCN) activity and closure analysis at the HKUST Supersite in Hong Kong, Atmos. Chem. Phys., 14, 10267-10282, doi:https://doi.org/10.5194/acp-14-10267-2014, 2014.

Moore, R. H., Nenes, A., and Medina, J.: Scanning Mobility CCN Analysis-A Method for Fast Measurements of Size-Resolved CCN Distributions and Activation Kinetics, Aerosol Sci Tech, 44, 861-871, doi:https://doi.org/10.1080/02786826.2010.498715, 2010.

Ou, H., Cai, M., Zhang, Y., Ni, X., Liang, B., Sun, Q., Mai, S., Sun, C., Zhou, S., Wang, H., Sun, j., and Zhao, J.: Measurement Report: Seasonal variation and anthropogenic influence on cloud condensation nuclei (CCN) activity in the South China Sea: Insights from shipborne observations during summer and winter of 2021 [dataset], doi:https://doi.org/10.6084/m9.figshare.25472545, 2024.

Ovadnevaite, J., Zuend, A., Laaksonen, A., Sanchez, K. J., Roberts, G., Ceburnis, D., Decesari, S., Rinaldi, M., Hodas, N., Facchini, M. C., Seinfeld, J. H., and O' Dowd, C.: Surface tension prevails over solute effect in organic-influenced cloud droplet activation, Nature, 546, 637-641, doi:https://doi.org/10.1038/nature22806, 2017.

Patel, P. N. and Jiang, J. H.: Cloud condensation nuclei characteristics at the Southern Great Plains site: role of particle size distribution and aerosol hygroscopicity, Environ Res Commun, 3, doi:https://doi.org/10.1088/2515-7620/ac0e0b, 2021.

Petters, M. D. and Kreidenweis, S. M.: A single parameter representation of hygroscopic growth and cloud condensation nucleus activity, Atmos. Chem. Phys., 7, 1961-1971, doi:https://doi.org/10.5194/acp-7-1961-2007, 2007.

Pöhlker, M. L., Pöhlker, C., Ditas, F., Klimach, T., Hrabe de Angelis, I., Araújo, A., Brito, J., Carbone, S., Cheng, Y., Chi, X., Ditz, R., Gunthe, S. S., Kesselmeier, J., Könemann, T., Lavrič, J. V., Martin, S. T., Mikhailov, E., Moran-Zuloaga, D., Rose, D., Saturno, J., Su, H., Thalman, R., Walter, D., Wang, J., Wolff, S., Barbosa, H. M. J., Artaxo, P., Andreae, M. O., and Pöschl, U.: Long-term observations of cloud

Formatted: Font: (Asian) +Body Asian (等线)

condensation nuclei in the Amazon rain forest – Part 1: Aerosol size distribution, hygroscopicity, and new model parametrizations for CCN prediction, Atmos. Chem. Phys., 16, 15709-15740, doi:https://doi.org/10.5194/acp-16-15709-2016, 2016.

Qin, Y., Wang, H., Wang, Y., Lu, X., Tang, H., Zhang, J., Li, L., and Fan, S.: Wildfires in Southeast Asia pollute the atmosphere in the northern South China Sea, Sci Bull (Beijing), 69, 1011-1015, doi:https://doi.org/10.1016/j.scib.2024.02.026, 2024.

Quinn, P. K., Bates, T. S., Coffman, D. J., and Covert, D. S.: Influence of particle size and chemistry on the cloud nucleating properties of aerosols, Atmos. Chem. Phys., 8, 1029-1042, doi:https://doi.org/10.5194/acp-8-1029-2008, 2008.

Quinn, P. K., Bates, T. S., Coffman, D. J., Upchurch, L., Johnson, J. E., Moore, R., Ziemba, L., Bell, T. G., Saltzman, E. S., Graff, J., and Behrenfeld, M. J.: Seasonal Variations in Western North Atlantic Remote Marine Aerosol Properties, J Geophys Res-Atmos, 124, 14240-14261, doi:https://doi.org/10.1029/2019jd031740, 2019.

Rose, D., Nowak, A., Achtert, P., Wiedensohler, A., Hu, M., Shao, M., Zhang, Y., Andreae, M. O., and Poschl, U.: Cloud condensation nuclei in polluted air and biomass burning smoke near the mega-city Guangzhou, China - Part 1: Size-resolved measurements and implications for the modeling of aerosol particle hygroscopicity and CCN activity, Atmos. Chem. Phys., 10, 3365-3383, doi:https://doi.org/10.5194/acp-10-3365-2010, 2010.

Ross, K. E., Piketh, S. J., Bruintjes, R. T., Burger, R. P., Swap, R. J., and Annegarn, H. J.: Spatial and seasonal variations in CCN distribution and the aerosol-CCN relationship over southern Africa, J Geophys Res-Atmos, 108, doi:https://doi.org/10.1029/2002jd002384, 2003.

Safai, P. D., Raju, M. P., Rao, P. S. P., and Pandithurai, G.: Characterization of carbonaceous aerosols over the urban tropical location and a new approach to evaluate their climatic importance, Atmos Environ, 92, 493-500, doi:https://doi.org/10.1016/j.atmosenv.2014.04.055, 2014.

Sarangi, B., Ramachandran, S., Rajesh, T. A., and Dhaker, V. K.: Black carbon linked aerosol hygroscopic growth: Size and mixing state are crucial, Atmos Environ., 200, 110-118, doi:https://doi.org/https://doi.org/10.1016/j.atmosenv.2018.12.001, 2019.

Schmale, J., Henning, S., Decesari, S., Henzing, B., Keskinen, H., Sellegri, K., Ovadnevaite, J., Pohlker, M. L., Brito, J., Bougiatioti, A., Kristensson, A., Kalivitis, N., Stavroulas, I., Carbone, S., Jefferson, A., Park, M., Schlag, P., Iwamoto, Y., Aalto, P., Aijala, M., Bukowiecki, N., Ehn, M., Frank, G., Frohlich, R.,

Formatted: Normal

Formatted: Font: (Asian) +Body Asian (等线)

Deleted: Roldin, P., Ehn, M., Kurtén, T., Olenius, T., Rissanen, M. P., Sarnela, N., Elm, J., Rantala, P., Hao, L., Hyttinen, N., Heikkinen, L., Worsnop, D. R., Pichelstorfer, L., Xavier, C., Clusius, P., Öström, E., Petäjä, T., Kulmala, M., Vehkamäki, H., Virtanen, A., Riipinen, I., and Boy, M.: The role of highly oxygenated organic molecules in the Boreal aerosol-cloud-climate system, Nat. Commun, 10, 4370, doi:https://doi.org/10.1038/s41467-019-12338-8, 2019.

Formatted: Normal

Formatted: Font: (Asian) +Body Asian (等线)

Deleted: Savoie, D. L., Arimoto, R., Keene, W. C., Prospero, J. M., Duce, R. A., and Galloway, J. N.: Marine biogenic and anthropogenic contributions to non-sea-salt sulfate in the marine boundary layer over the North Atlantic Ocean, J Geophys Res-Atmos, 107, doi:https://doi.org/10.1029/2001jd000970, 2002.

Frumau, A., Herrmann, E., Herrmann, H., Holzinger, R., Kos, G., Kulmala, M., Mihalopoulos, N., Nenes, A., O'Dowd, C., Petaja, T., Picard, D., Pohlker, C., Poschl, U., Poulain, L., Prevot, A. S. H., Swietlicki, E., Andreae, M. O., Artaxo, P., Wiedensohler, A., Ogren, J., Matsuki, A., Yum, S. S., Stratmann, F., Baltensperger, U., and Gysel, M.: Long-term cloud condensation nuclei number concentration, particle number size distribution and chemical composition measurements at regionally representative observatories, Atmos. Chem. Phys., 18, 2853-2881, doi:https://doi.org/10.5194/acp-18-2853-2018, 2018.

Seinfeld, J. H. and Pandis, S. N.: Atmospheric Chemistry and Physics: From Air Pollution to Climate Change, Wiley2016.

Sihto, S. L., Mikkila, J., Vanhanen, J., Ehn, M., Liao, L., Lehtipalo, K., Aalto, P. P., Duplissy, J., Petaja, T., Kerminen, V. M., Boy, M., and Kulmala, M.: Seasonal variation of CCN concentrations and aerosol activation properties in boreal forest, Atmos. Chem. Phys., 11, 13269-13285, doi:https://doi.org/10.5194/acp-11-13269-2011, 2011.

Sun, Q., Liang, B., Cai, M., Zhang, Y., Ou, H., Ni, X., Sun, X., Han, B., Deng, X., Zhou, S., and Zhao, J.: Cruise observation of the marine atmosphere and ship emissions in South China Sea: Aerosol composition, sources, and the aging process, Environ. Pollut, 316, 120539, doi:https://doi.org/10.1016/j.envpol.2022.120539, 2023.

Wang, B., Huang, F., Wu, Z., Yang, J., Fu, X., and Kikuchi, K.: Multi-scale climate variability of the South China Sea monsoon: A review, Dynam Atmos Oceans, 47, 15-37, doi:https://doi.org/10.1016/j.dynatmoce.2008.09.004, 2009.Wang, Y., Chen, J., Wang, Q., Qin, Q., Ye, J., Han, Y., Li, L., Zhen, W., Zhi, Q., Zhang, Y., and Cao, J.: Increased secondary aerosol contribution and possible processing on polluted winter days in China, Environ Int, 127, 78-84, doi:https://doi.org/10.1016/j.envint.2019.03.021, 2019.

Wang, Y. Q.: MeteoInfo: GIS software for meteorological data visualization and analysis, Meteorol. Appl, 21, 360-368, doi:https://doi.org/10.1002/met.1345, 2014.

Xiao, H.-W., Xiao, H.-Y., Luo, L., Shen, C.-Y., Long, A.-M., Chen, L., Long, Z.-H., and Li, D.-N.: Atmospheric aerosol compositions over the South China Sea: temporal variability and source apportionment, Atmos. Chem. Phys., 17, 3199-3214, doi:https://doi.org/10.5194/acp-17-3199-2017, 2017.

Deleted: Siegel, K., Neuberger, A., Karlsson, L., Zieger, P., Mattsson, F., Duplessis, P., Dada, L., Daellenbach, K., Schmale, J., Baccarini, A., Krejci, R., Svenningsson, B., Chang, R., Ekman, A. M. L., Riipinen, I., and Mohr, C.: Using Novel Molecular-Level Chemical Composition Observations of High Arctic Organic Aerosol for Predictions of Cloud Condensation Nuclei, Environ. Sci. Technol, 56, 13888-13899, doi:https://doi.org/10.1021/acs.est.2c02162, 2022.

Deleted: Tao, J., Kuang, Y., Ma, N., Hong, J., Sun, Y., Xu, W., Zhang, Y., He, Y., Luo, Q., Xie, L., Su, H., and Cheng, Y.: Secondary aerosol formation alters CCN activity in the North China Plain, Atmos. Chem. Phys., 21, 7409-7427, doi:https://doi.org/10.5194/acp-21-7409-2021, 2021.
Topping, D. O., McFiggans, G. B., and Coe, H.: A curved multi-component aerosol hygroscopicity model framework: Part 1 - Inorganic compounds, Atmos. Chem. Phys., 5, 1205-1222, doi:https://doi.org/10.5194/acp-5-1205-2005, 2005.

Formatted: Font: (Asian) +Body Asian (等线)

Deleted: Tseng, Y. L., Yuan, C. S., Bagtasa, G., Chuang, H. L., and Li, T. C.: Inter-correlation of Chemical Compositions, Transport Routes, and Source Apportionment Results of Atmospheric PM2.5 in Southern Taiwan and the Northern Philippines, Aerosol Air Qual Res, 19, 2645-2661, doi:https://doi.org/10.4209/aaqr.2019.10.0526, 2019.

Formatted: Indent: Left: 0 cm

Deleted:

Formatted: 参考文献

Deleted:

Deleted: Weingartner, E., Burtscher, H., and Baltensperger, U.: Hygroscopic properties of carbon and diesel soot particles, Atmos Environ, 31, 2311-2327, doi:https://doi.org/10.1016/S1352-2310(97)00023-X, 1997.
Wu, C. and Yu, J. Z.: Determination of primary combustion source organic carbon-to-elemental carbon (OCaEuro-/aEuro-EC) ratio using ambient OC and EC measurements: secondary OC-EC correlation minimization method, Atmos. Chem. Phys., 16, 5453-5465, doi:https://doi.org/10.5194/acp-16-5453-2016, 2016.

Formatted: Normal

Formatted: Font: (Asian) +Body Asian (等线)

Deleted: Yang, M., Jalava, P., Wang, X.-F., Bloom, M. S., Leskinen, A., Hakkarainen, H., Roponen, M., Komppula, M., Wu, Q.-Z., Xu, S.-L., Lin, L.-Z., Liu, R.-Q., Hu, L.-W., Yang, B.-Y., Zeng, X.-W., Yu, Y.-J., and Dong, G.-H.: Winter and spring variation in sources, chemical components and toxicological responses of urban air particulate matter samples in Guangzhou, China, Sci. Total Environ, 845, 157382, doi:https://doi.org/10.1016/j.scitotenv.2022.157382, 2022.
Zhang, X. Y., Zhuang, G. S., Guo, J. H., Yin, K. D., and Zhang, P.: Characterization of aerosol over the Northern South China Sea during two cruises in 2003, Atmos Environ, 41, 7821-7836, doi:https://doi.org/10.1016/j.atmosenv.2007.06.031, 2007.
Zheng, G. J., Kuang, C. G., Uin, J., Watson, T., and Wang, J.: Large contribution of organics to condensational growth and formation of cloud condensation nuclei (CCN) in the remote marine boundary layer, Atmos. Chem. Phys., 20, 12515-12525, doi:https://doi.org/10.5194/acp-20-12515-2020, 2020.

Table 1. The number concentration of particle and cloud condensation nuclei at different supersaturation (SS), the hygroscopicity and activation ratio (AR) at different SS in different studies.

Location	period	N_{CN} (cm^{-3})	N_{CCN} (cm^{-3})	Hygroscopicity (κ)	AR	Reference
South China Sea	2021.05.05-2021.06.09	6966±9249	2019±2993 (0.20% SS) 4445±7018 (0.40% SS) 4786±6402 (0.70% SS)	0.49±0.42 (0.20% SS) 0.74±0.51 (0.40% SS)	0.43±0.17 (0.20% SS) 0.68±0.19 (0.40% SS) 0.89±0.12 (0.70% SS)	This study
Northern South China Sea	2021.12.19-2021.12.29	4988±3474	1100±1287 (0.10% SS) 1678±1046 (0.20% SS) 2346±1767 (0.40% SS) 2921±1917 (0.70% SS)	0.50±0.21 (0.10% SS) 0.31±0.10 (0.20% SS) 0.19±0.05 (0.40% SS) 0.15±0.05 (0.70% SS)	0.23±0.10 (0.10% SS) 0.35±0.12 (0.20% SS) 0.48±0.14 (0.40% SS) 0.60±0.16 (0.70% SS)	This study
Northern South China Sea	2018.8.6-2018.8.27	3463	1544 (0.34% SS)	0.38±0.09 (0.18% SS) 0.40±0.08 (0.34% SS) 0.38±0.08 (0.59% SS)	/	Cai et al., 2020
Remote South China Sea	2012.9.14-2012.9.26	503±455	450±388 (0.14% SS) 675±516 (0.38% SS) 698±555 (0.53% SS) 724±512 (0.71% SS)	0.54±0.14 (0.14% SS) 0.50±0.21 (0.38% SS)	0.47±0.16 (0.14% SS) 0.72±0.17 (0.38% SS) 0.79±0.15 (0.53% SS) 0.85±0.13 (0.71% SS)	Atwood et al., 2017
Western North Pacific	2015.3.4-2015.3.26	/	/	0.75±0.21 (0.11% SS) 0.51±0.16 (0.24% SS) 0.45±0.16 (0.60% SS)	0.40±0.22 (0.11% SS) 0.50±0.22 (0.24% SS) 0.70±0.23 (0.60% SS)	Kawana et al., 2020
Guangzhou	2014.11-2014.12	/	3103±1913 (0.10% SS) 5095±2972 (0.20% SS) 6524±3783 (0.40% SS)	0.37±0.11 (0.10% SS) 0.29±0.09 (0.20% SS) 0.18±0.07 (0.40% SS)	0.26±0.10 (0.10% SS) 0.41±0.14 (0.20% SS) 0.53±0.15 (0.40% SS)	Cai et al., 2018

Formatted Table

	7913±4234 (0.70% SS)	0.15±0.06 (0.70% SS)	0.64±0.13 (0.70% SS)

1272

Table 2. The number concentration of particle and cloud condensation nuclei in different periods.

	Summer			Winter		
Cluster	Indochinese Peninsula	Luzon	Marine	Mainland China	Marine	Mixed
N_{CCN} (cm^{-3})						
0.1% SS	\	\	\	1460±1670	464±243	929±444
0.2% SS	1290±785	4093±4864	1112±682	2105±974	649±362	1499±548
0.4% SS	1634±1121	8241±7478	1885±1142	3014±1934	831±439	1900±696
0.7% SS	1968±1111	10776±10540	2477±1541	3668±1841	1052±493	2296±829
N_{CN} (cm^{-3})						
Total	2699±2147	14674±13844	3033±2366	6875±3263	1728±465	2918±1204
Nucleation	111±206	1543±3341	238±426	893±925	214±281	141±191
Aikten	1156±1261	8653±8815	1668±1526	3089±2017	732±337	806±427
Accumulation	1434±1444	3764±4157	1121±929	2923±2440	781±313	1975±831

Table 3. The slope and coefficient of determination (in parentheses) in CCN closure analysis at different supersaturations in different periods.

	Summer			Winter		
Cluster	Luzon	Indochinese Peninsula	Marine	Mainland China	Mixed	Marine
Internal scheme						
0.1% SS	\	\	\	0.81 (0.94)	0.64 (0.92)	0.65 (0.95)
0.2% SS	0.82 (0.82)	0.73 (0.80)	0.79 (0.91)	1.05 (0.96)	0.93 (0.97)	0.79 (0.89)
0.4% SS	0.79 (0.92)	0.76 (0.62)	0.80 (0.92)	1.23 (0.97)	1.04 (0.98)	1.01 (0.95)

Formatted: Font: (Asian) +Body Asian (等线)

Deleted: Page Break

0.7% SS	0.80 (0.88)	0.85 (0.52)	0.80 (0.90)	1.26 (0.97)	1.06 (0.99)	0.97 (0.91)
External scheme						
0.1% SS	\	\	\	0.97 (0.95)	0.96 (0.92)	0.97 (0.95)
0.2% SS	0.73 (0.83)	0.63 (0.76)	0.75 (0.90)	0.98 (0.96)	0.99 (0.97)	0.94 (0.89)
0.4% SS	0.69 (0.85)	0.69 (0.65)	0.74 (0.91)	0.99 (0.97)	0.99 (0.98)	0.97 (0.95)
0.7% SS	0.70 (0.85)	0.80 (0.53)	0.72 (0.88)	0.99 (0.97)	0.99 (0.99)	0.96 (0.92)

279
280

Formatted: Font: (Asian) +Body Asian (等线), Check spelling and grammar

FIGURE CAPTION

Figure 1. The cruises of two shipborne observations, and the location of sample line and chimney of Tan Kah Kee, and Sun Yat-sen scientific vessel (a); Wind rose of the wind direction and wind speed in summer and winter cruises; The radius represents the frequency of wind direction occurrences, and the shaded areas indicate wind speed (b) and (c).

Figure 2. Timeseries of (a) particle number size distribution, (b) mass concentration of NR-PM_1, and (c) its fraction, (d) mass concentration of organic carbon and elemental carbon, (e) number concentration of total particle and cloud condensation nuclei under the supersaturation of 0.1%, 0.2%, 0.4%, and 0.7%, and (f) aerosol hygroscopicity. The number 1 in figure number means timeseries in summer and number 2 means it in winter.

Figure 3. Particle number size distribution in summer (a) and winter (b); The red markers represent the activation diameters and hygroscopicity parameters corresponding to 0.1%, 0.2%, 0.4%, and 0.7% supersaturations in this study (without 0.1% in summer). The green markers represent the hygroscopicity parameters reported in Atwood et al. (2017) for the southern South China Sea during summer. The gray markers represent the hygroscopicity parameters documented in Cai et al. (2018) for the Pearl River Delta region during winter. The fraction of NR-PM_1 in summer (c) and winter (d) in this study, in northern SCS reported by Liang et al. (2021), and in North Pacific reported by Choi et al. (2017).

Figure 4. The cluster analysis result in summer (a), and winter (b). The solid line in summer means cluster analysis from May 5 to May 24 and the dash line in summer means cluster analysis from May 25 to June 9; The solid line in winter means cluster analysis from Dec 19 to Dec 21 and Dec 27 to Dec 29, and the dash line in winter means cluster analysis from Dec 22 to Dec 26.

Figure 5. The fraction of NR-PM_1 in "Luzon" period (a), "Indochinese Peninsula" period (b), and "Marine-s" period (c) in summer. The fraction of NR-PM_1 in "Mainland China" period (d), "Mixed" period (e), and "Marine-w" period (f) in winter.Figure 6. The particle number size distribution (PNSD) in "Luzon" period (a), "Indochinese Peninsula" period (b), and "Marine-s" period (c) in summer. The PNSD in "Mainland China" period (d), "Mixed" period (e), and "Marine-w" period (f) in winter.Figure 7. The activation ratio (AR) at different supersaturation (SS) in different periods (a); The aerosol hygroscopicity at different supersaturation (SS) in different periods (b).Figure 8. The normalized mean bias (NMB) calculated by "Internal-mixed" scheme and "External-mixed" scheme according to CCN

Deleted: cruies

Deleted: observation

Formatted: Subscript

Deleted: under effect of terrestrial air masses

Deleted: Particle number size distribution under effect of mixed air masses in summer (c) and winter (d);

Formatted: Subscript

Deleted: The mass concentration of NR-PM1 , primary organic carbon, secondary carbon, elemental carbon, and black carbon and their fraction under effect of different air masses in summer and winter.
Figure 5. Scatter plot of κ under the supersaturation of 0.2% and organic mass fraction with linear regression.

Deleted: 6

Deleted: Activation ratio at supersaturation of 0.1%, 0.2%, 0.4%, and 0.7% under effect of terrestrial and mixed air masses in summer and winter. The box extends from the first quartile (Q1) to the third quartile (Q3) of the data, with a line at the median. The box extends from Q1 to Q3 of the data, with a line at the median. The whiskers extend from the box by 1.5 times of the inter-quartile range (IQR). Flier points are those passing the end of the whiskers.

Formatted: Subscript

Deleted:

Deleted: 7

Deleted: Differences in activation fraction calculated from different particle size distributions and activation diameters.

Deleted: 8

Deleted: Variations of κSS:0.4%, trace gases (NOx and CO), OC/EC, BC, SOC/OC, mass fraction of NR-PM1 chemical composition, as well as number concentrations of nucleation mode, Aitken mode, and accumulation mode with offshore distance under effect of terrestrial and mixed air masses in summer and winter.

Deleted: 9

closure method. The marker of circle means “Internal-mixed” scheme and the marker of triangle means “External-mixed” scheme. Different colors means different supersaturations.

Deleted: The difference between the calculated cloud condensation nuclei number concentration (NCCN) using the D50 from the farthest and nearest offshore distances, along with the measured particle number size distribution (PNSD), and the measured NCCN under the effect of terrestrial air masses in summer (a1 and a2) and winter (c1 and c2); The difference between the calculated NCCN using the PNSD from the farthest and nearest offshore distances, along with the measured D50, and the measured NCCN under the effect of terrestrial air masses in summer (b1 and b2) and winter (d1 and d2). ΔNCCN refers to the difference between calculated NCCN and observed NCCN, divided by the observed NCCN.

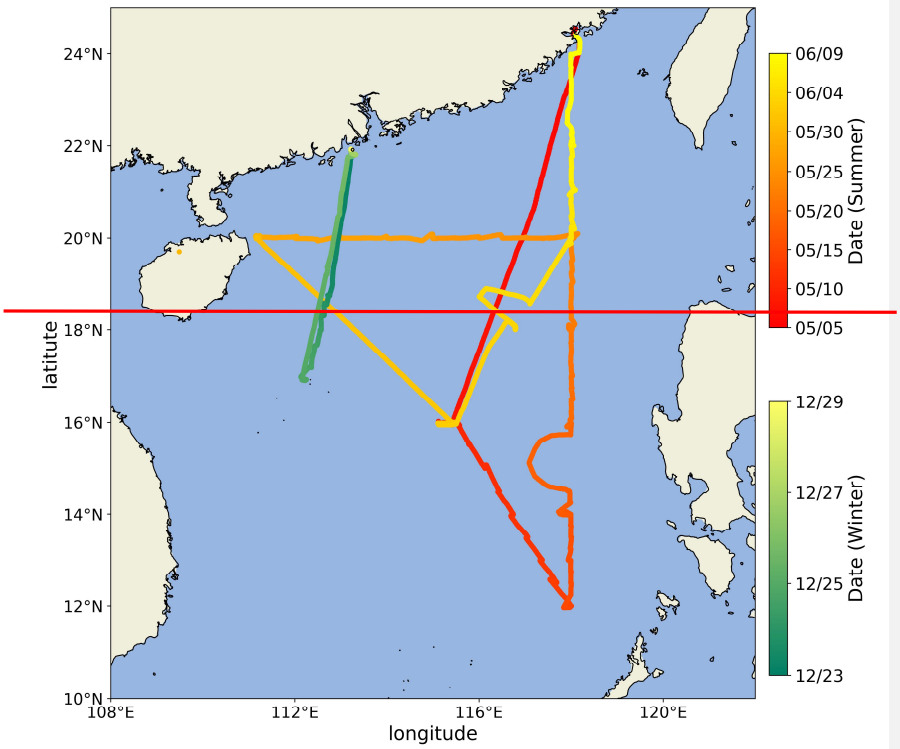
24°N
22°N
20°N
18°N
16°N
14°N
12°N
10°N
latitute
108°E
112°E
116°E
120°E
longitude
06/09
06/04
05/30
05/25
05/20
05/15
05/10
05/05
Date (Summer)
12/29
12/27
12/25
12/23
Date (Winter)

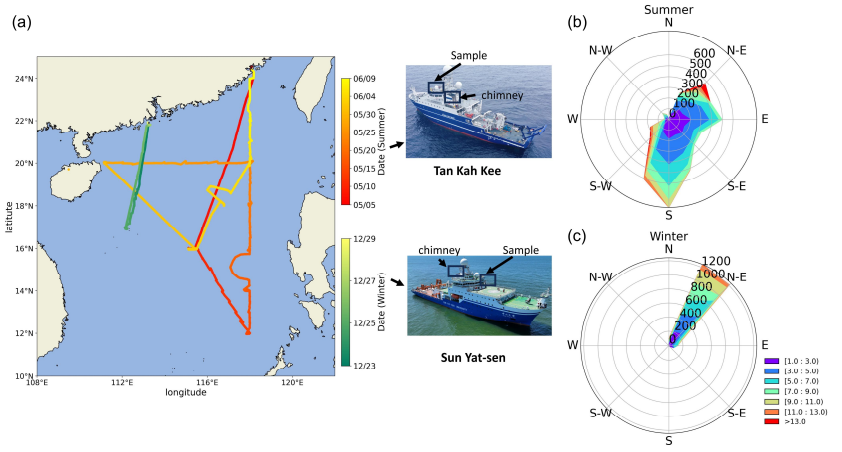
(a)
Sample
chimney
Tan Kah Kee
chimney
Sample
Sun Yat-sen
(b)
Summer
N
N-E
E
S-E
S
S-W
W
N-W
600
500
400
300
200
100
0
(c)
Winter
1200
1000
800
600
400
200
[1.0 : 3.0)
[3.0 : 5.0)
[5.0 : 7.0)
[7.0 : 9.0)
[9.0 : 11.0)
[11.0 : 13.0)
>13.0

Fig. 1

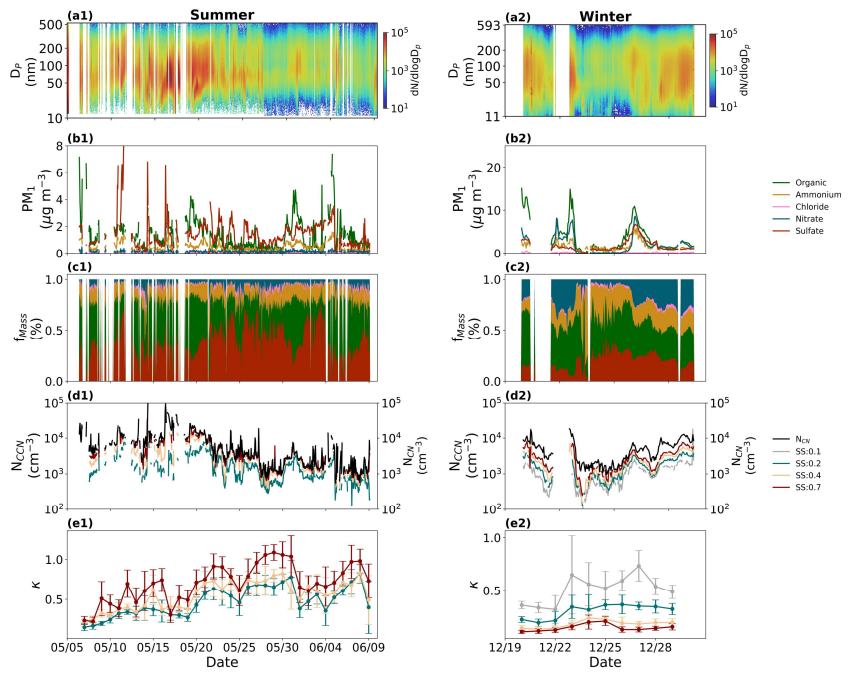

Fig. 2

Deleted:

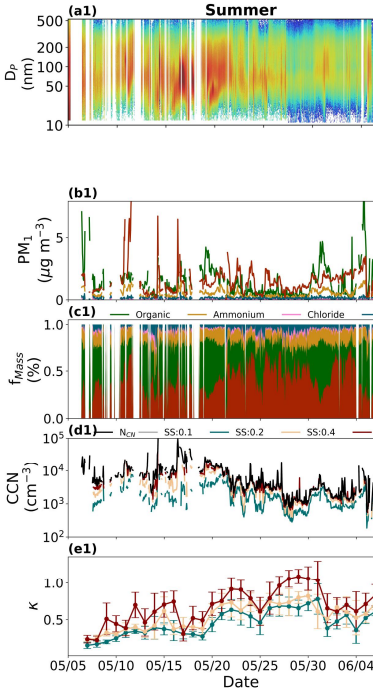

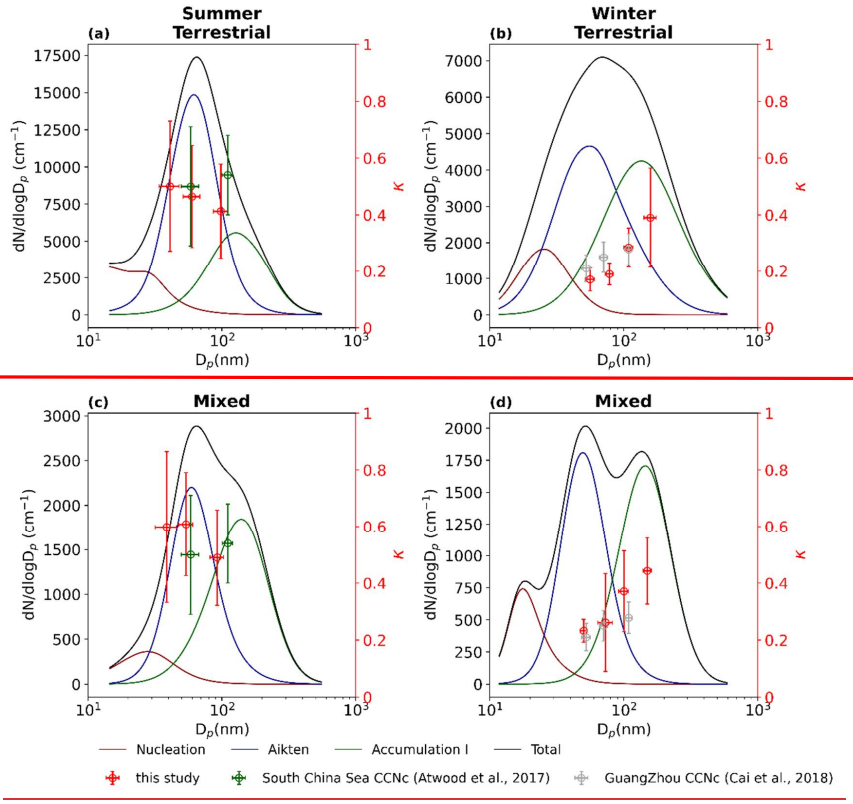
Summer
Terrestrial
(a)
Winter
Terrestrial
(b)
Mixed
(c)
Mixed
(d)
dN/dlogD$_p$ (cm^{-3})
κ
D$_p$(nm)
Nucleation
Aikten
Accumulation I
Total
this study
South China Sea CCNc (Atwood et al., 2017)
GuangZhou CCNc (Cai et al., 2018)

1368

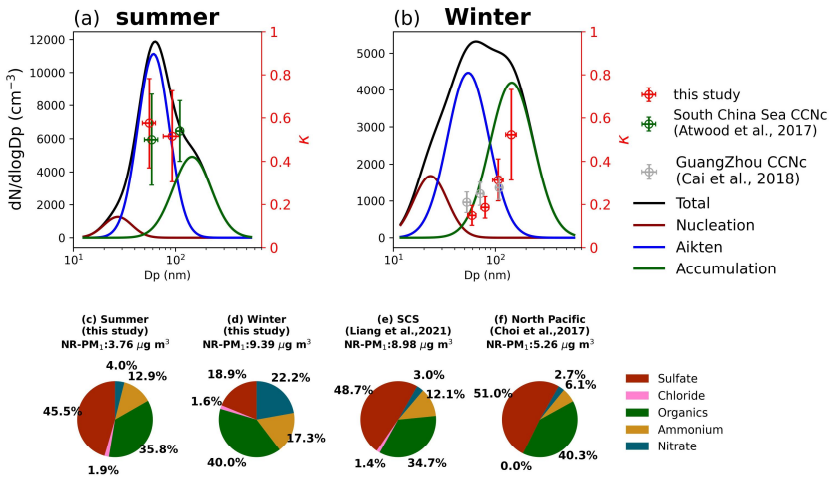

Fig. 3

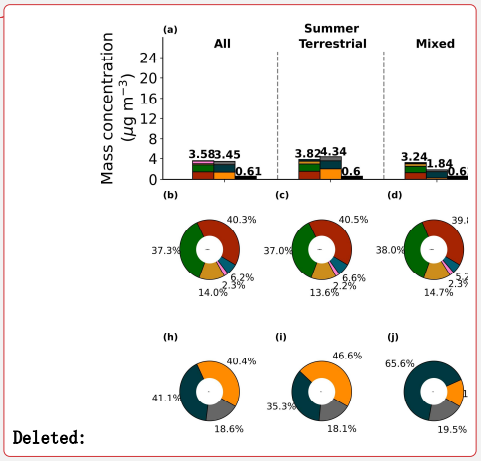

Deleted:

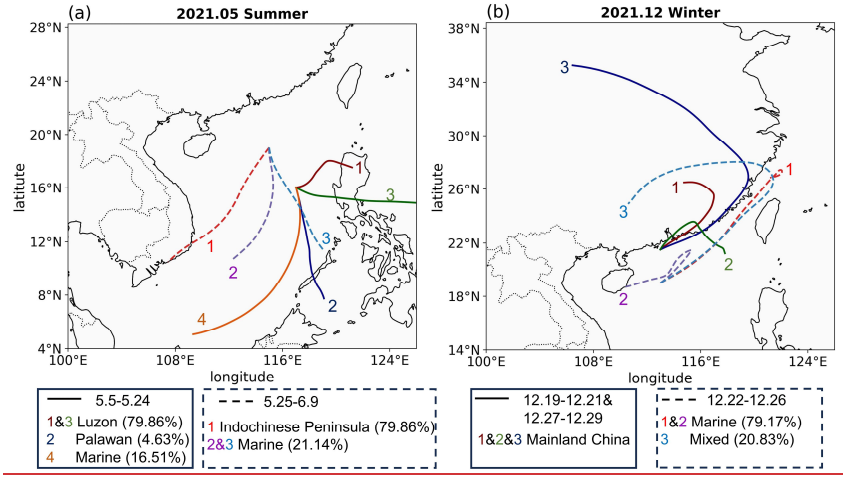
(a)
2021.05 Summer
(b)
2021.12 Winter
latitude
longitude
28°N
24°N
20°N
16°N
12°N
8°N
4°N
38°N
34°N
30°N
26°N
22°N
18°N
14°N
100°E
108°E
116°E
124°E
5.5-5.24
1&3 Luzon (79.86%)
2 Palawan (4.63%)
4 Marine (16.51%)
5.25-6.9
1 Indochinese Peninsula (79.86%)
2&3 Marine (21.14%)
12.19-12.21&
12.27-12.29
1&2&3 Mainland China
12.22-12.26
1&2 Marine (79.17%)
3 Mixed (20.83%)

Fig. 4

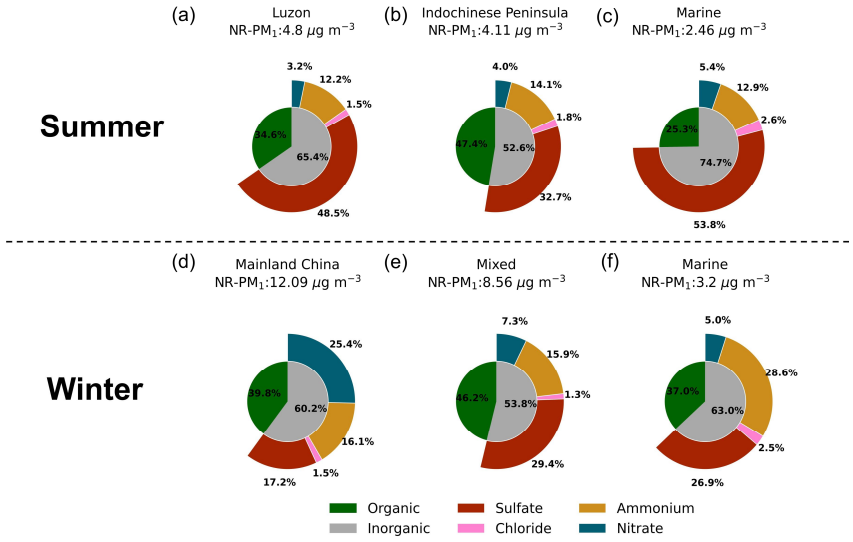

Fig.5

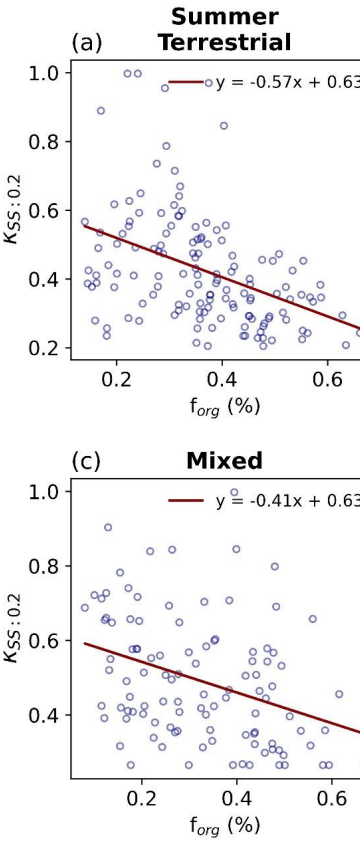

Deleted:

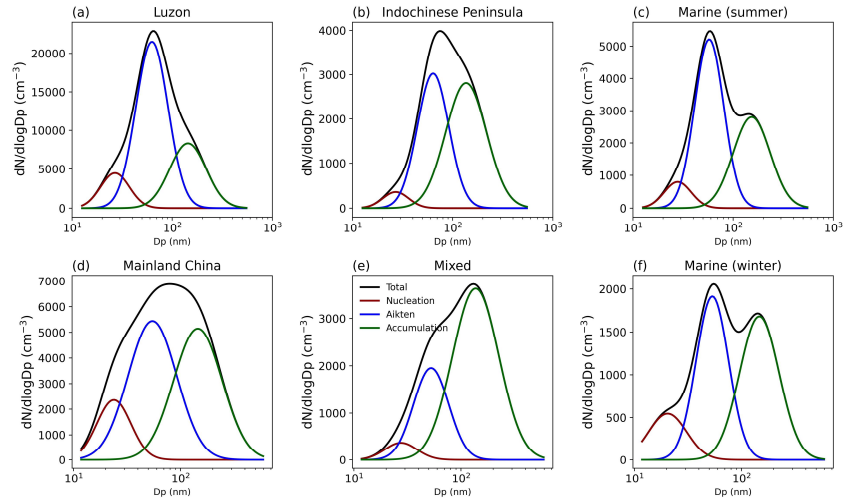

Fig. 6

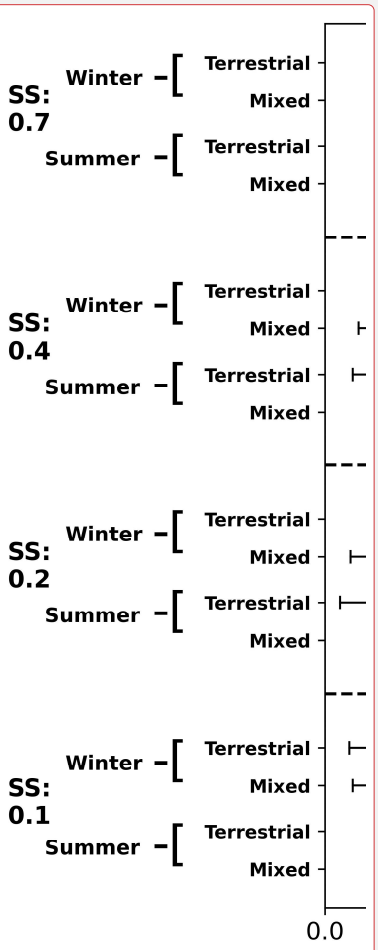

Deleted:

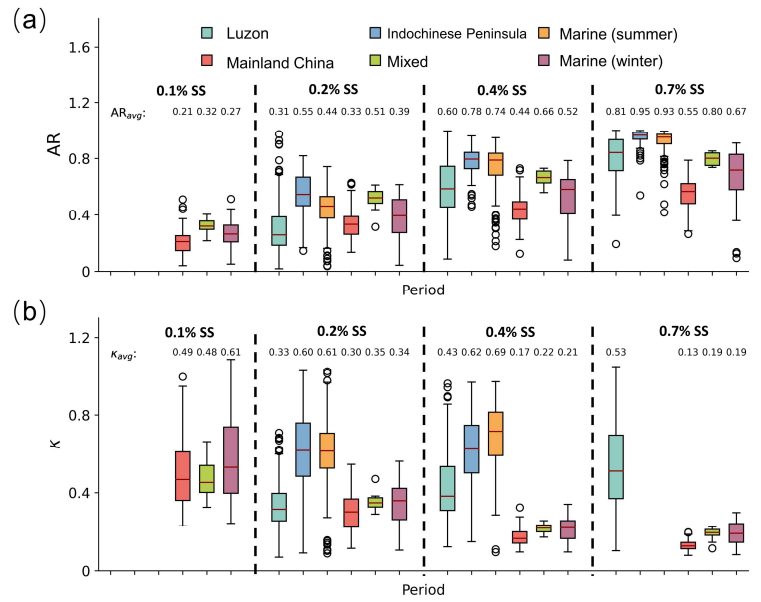

Fig. 7

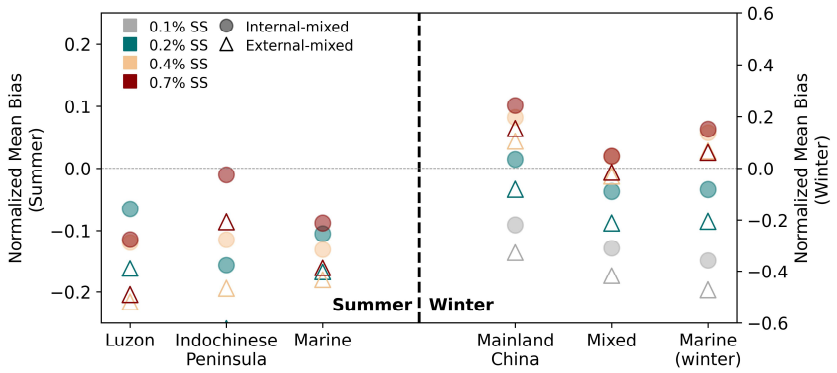

Fig. 8

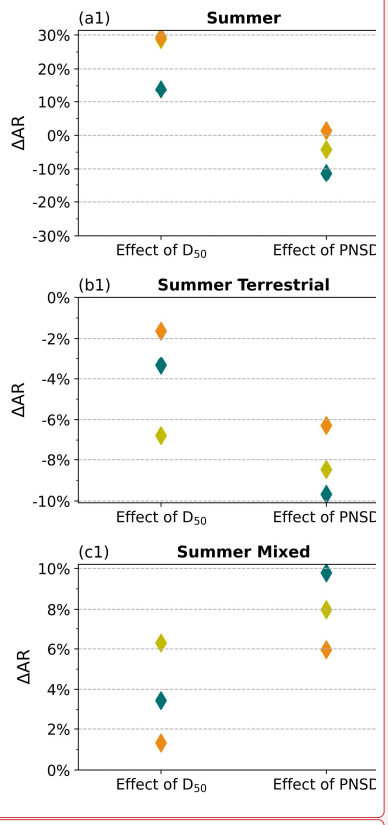

Deleted:

Deleted:

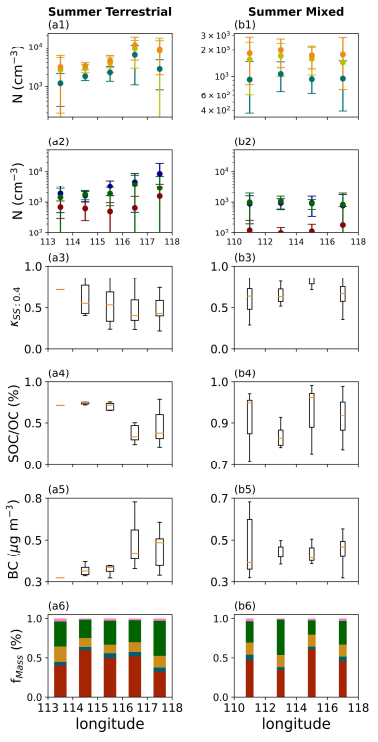

Deleted:

399
400

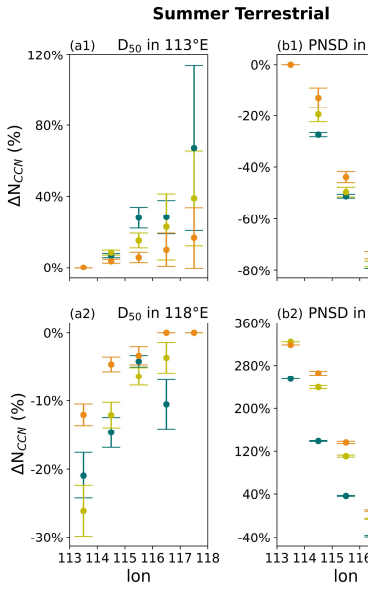

Deleted:

Fig. 9

404
1405
1406
1407

Deleted: Sarangi, B., Ramachandran, S., Rajesh, T. A., and Dhaker, V. K.: Black carbon linked aerosol hygroscopic growth: Size and mixing state are crucial, Atmos Environ., 200, 110-118, doi:https://doi.org/https://doi.org/10.1016/j.atmosenv.2018.12.001, 2019. ... [4]

Page 11: [1] Deleted 区恒嘉 2024-7-18 0:57:00

Page 14: [2] Deleted 区恒嘉 2024-7-30 23:05:00

Page 16: [3] Deleted 区恒嘉 2024-7-20 23:10:00

Page 40: [4] Deleted 区恒嘉 2024-7-28 0:37:00